PROCEEDINGS A

royalsocietypublishing.org/journal/rspa

Research

Check for updates

Article submitted to journal

Subject Areas:

glaciology, ice sheet modelling

Keywords:

Antarctica, ice sheet dynamics

Author for correspondence:

F. S. McCormack e-mail: felicity.mccormack@monash.edu

Synthetic bed topographies for Antarctica and their utility in ice sheet modelling

Felicity S. McCormack[1], Tobias Stål[2,3], Niya Shao[4], Emma MacKie[4], Ana Fabela Hinojosa[1], Mareen Lösing[3,5], Jason L. Roberts[6,7], Shivani Ehrenfeucht[8], Christine F. Dow[9]

[1]Securing Antarctica's Environmental Future, School of Earth, Atmosphere & Environment, Monash University, Clayton, Kulin Nations, Victoria, Australia
[2]School of Natural Sciences (Physics), University of Tasmania, Tasmania, Australia. [3]The Australian Centre for Excellence in Antarctic Science (ACEAS)
[4]Department of Geological Sciences, University of Florida, Gainesville, Florida, USA
[5]School of Earth and Oceans, University of Western Australia, Perth, Western Australia, Australia
[6]Australian Antarctic Division, Kingston, Tasmania, Australia
[7]Australian Antarctic Program Partnership, Institute for Marine and Antarctic Studies, University of Tasmania, Hobart, Tasmania, Australia
[8]Potsdam Institute for Climate Impact Research, Potsdam, Germany
[9]Department of Geography & Environmental Management, University of Waterloo, Waterloo, Ontario, Canada

Bed topography is a key control on the evolution of the Antarctic Ice Sheet, influencing ice flow, grounding line retreat, and the rate and timing of ice mass loss. To assess the sensitivity of ice sheet evolution to bed variability in ice sheet models, synthetic gridded bed topography datasets are often used. Here, we review methods commonly used to generate synthetic beds, their associated uncertainties, and the influence of the approach on the characteristics of the resulting bed. Using the Aurora Subglacial Basin in East Antarctica

THE ROYAL SOCIETY PUBLISHING

as a case study, we evaluate the impact of five synthetic bed generation methods on projected ice mass loss under a high emission scenario. Sea level rise estimates vary by up to 11% when basal friction coefficients from the friction law are optimised for each bed, and by up to 23% when using non-optimised coefficients. Our results highlight the importance of relatively small bed variations on the timing and extent of grounding line retreat, and the need for process-informed representation of the basal friction in decadal- to centennial-scale sea level projections.

1. Introduction

Bed topography is one of the most critical variables for controlling the evolution of the Antarctic Ice Sheet. At regional- to sector-scale, bed topography controls the magnitude and timing of ice volume changes by influencing the ice velocity and rate of grounding line retreat. This influence can be due to the role of pinning points [1–5], or via the bed slope or curvature that influence glacier susceptibility to instabilities [6–9]. Ice-bed interactions provide resistance to flow [10], including through pinning points [11], influencing buttressing [12,13] and determining the relative contributions of deformation and sliding to the overall column-averaged speed [14–16]. Frictional heating at the base of the ice sheet regulates the basal thermal regime [17] and production of liquid meltwater, which feeds the subglacial hydrological system [18–22]. Sub-ice shelf bathymetry influences the supply of ocean water masses to the ice shelf cavity [23,24], and ice shelf and grounding line ocean-driven melt rates [25,26]. Bed features influence the direction and magnitude (i.e. by modifying the total bed surface area) of heat transfer from the solid Earth to the ice sheet [27,28]. Bed topography is hence a critically important boundary condition for ice sheet dynamics, and by extension, numerical ice sheet modelling.

The primary method of measuring bed topography is via airborne radar surveys, which have provided over 82 million data points across Antarctica since the 1950s [29]. Ground-based radar and seismic surveys can also provide detailed bed measurements (e.g. [30,31]), but are highly localised and not as widely available as airborne radar. Hence, despite its importance, bed topography remains sparsely sampled across Antarctica, and particularly in critical regions: close to the present-day grounding line, and within upstream regions into which the grounding line may retreat in the coming decades to centuries. Compounding issues of insufficient survey coverage and radar reflections from off-target features in regions of steep topography – characteristic of deepened troughs in coastal zones – may lead to clutter, mask the ability to determine where the ice-bed interface is, and introduce uncertainties. Errors in the bed consequently propagate in ice sheet modelling simulations [32–34]. Bathymetry within ice shelf cavities is also particularly poorly known. These regions are inaccessible to most ship-borne platforms [35], and high fidelity sub-ice shelf submersible surveys are limited to small regions. While inversion of gravity data collected from airborne surveys provides some constraints on cavity bathymetry [36–39], large uncertainties in the density of the geological substrate may result in limited accuracy for the inferred cavity geometry. In addition, the limited achievable horizontal and vertical resolution of the gravity inversion impacts confidence in these estimates at the scales required for ocean modelling over broad regions (e.g. [36]).

Ice sheet modelling typically relies on gridded bed topography datasets that use some method of interpolation to gap-fill sparsely sampled radar-derived bed topography. However, the approach used to generate the bed topography influences how realistically features are captured in the resulting dataset. Some methods, such as Kriging, result in overly smooth beds, producing unrealistic estimates of topographic roughness [40,41], and can lead to large simulated mass flux divergence due to inconsistencies between model fields [34]. Alternative approaches to interpolating gridded bed topographies have been proposed to circumvent these issues. These encompass mass conservation, geostatistical simulation, and geophysical approaches (i.e.

gravity inversion in ice shelf cavities), or approaches that combine multiple methods or datasets, including machine learning. The resulting gridded bed topography datasets are "synthetic" in that they rely on different approaches to gap-fill or interpolate measured bed data.

The aim of this study is to examine the utility of synthetic bed topographies in ice sheet modelling applications. We define utility as allowing us to either accurately characterise ice sheet properties or dynamics (e.g. for studies that produce sea level rise projections) or to provide new insights into ice sheet processes that may be poorly understood. We first describe the objectives that guide the generation of synthetic bed topographies, reviewing the approaches used and how they assess uncertainty. Focusing on the Aurora Subglacial Basin, East Antarctica, we present an ice sheet modelling case study evaluating the sensitivity of projected sea level contributions to bed topographies generated using different approaches. We finish by discussing where such ensembles may be useful in constraining key unknowns in ice sheet modelling.

2. Methods to generate synthetic bed topographies

Synthetic topographies are typically generated to meet one of two primary objectives (figure 1): (i) to preserve elevation accuracy, ensuring the bed matches observed values where available and interpolates appropriately elsewhere; and (ii) to preserve statistical texture, such as covariance structure, so that roughness characteristics are spatially consistent. While these goals are not necessarily mutually exclusive (the true bed being an example that is both elevation- and texture-preserving), most methods prioritise one objective over the other to varying degrees. The utility of a given synthetic bed is influenced by its design objective, which in turn influences the types of ice sheet modelling questions it is most suited to be used for.

Below, we review common approaches for generating synthetic bed topographies, their placement along the elevation–texture spectrum, and the associated methods for estimating uncertainty.

(a) Traditional interpolation methods

(i) Mathematical approaches

Among the most straightforward approaches to generating synthetic bed topographies using non-geostatistical interpolation methods are mathematical functions used to gap-fill unsampled locations using nearby bed observations – i.e. generating elevation-preserving bed topographies. Interpolation methods include linear, inverse-distance weighted, spline, bilinear/bicubic, and nearest neighbour interpolation. No spatial model is assumed in these approaches, such that proximity to observations is the primary determinant of the resultant bed. Bed topography datasets generated using these approaches include: Bedmap1 [42], which uses inverse-cubed weighted algorithm; and Bedmap2 [43] and Bedmap3 [29,44], which use the Topo-to-raster method (formerly TopoGrid) from ANUDEM [45] implemented in ArcGIS. Topo-to-raster uses thin plate splines to produce a smooth surface through the use of iterative finite difference interpolation. Uncertainty in the interpolated topography in Bedmap3, which comprises 93% of the grounded ice, is calculated heuristically as a function of the distance to the closest topography measurement. This heuristic relationship between uncertainty and distance is derived from the difference between the new observations added in Bedmap3 and the interpolated topography in Bedmap2.

Many traditional approaches generate only a single bed realisation, where specific parameter choices can strongly influence the resulting topography. In such cases, uncertainties are typically addressed in an ad hoc or heuristic manner. To overcome these limitations, ensemble-based methods have been proposed that allow for more robust assessment and propagation of uncertainty. One such example is the Stochastic Meshless Uncertainty Gridding (SMUG, [46]) algorithm. SMUG is a point-wise interpolation scheme based on a local Taylor series, which produces a robust estimate of both the field being interpolated (here bed topography) and the

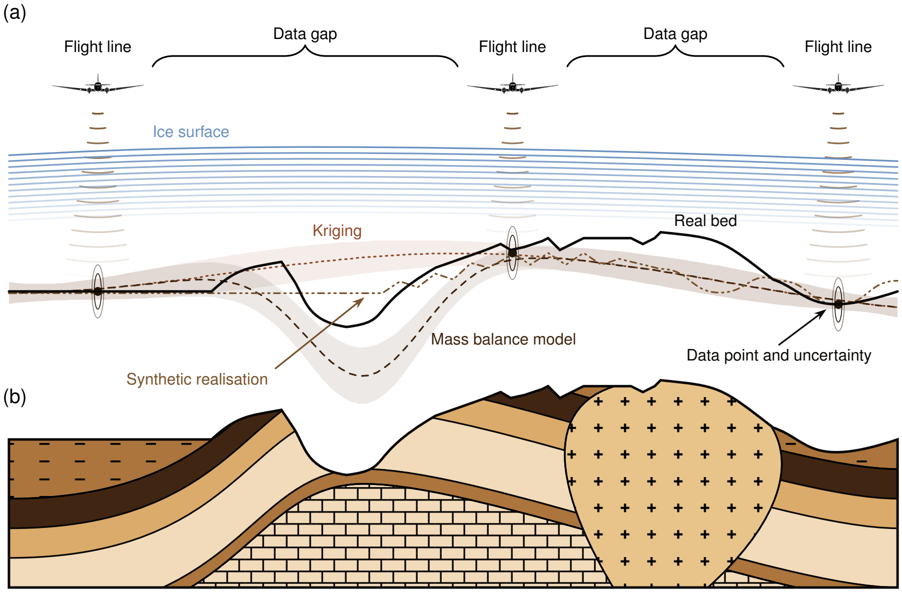

Figure 1. Schematic representing the information that is used to generate bed topographies. (a) Realisations of synthetic bed topographies in regions of data gaps between flight lines, highlighting differences between beds generated using: Kriging; mass conservation, which incorporates satellite observations of surface velocity; and geostatistical methods, which consider the shape of the bed at the flight lines. (b) Other information at the bed, including the bed type (e.g. hard or soft geological substrates) and the landforms formed by past subglacial and periglacial processes, which can influence both the generation of a synthetic bed topography, depending on the method used, as well as the evolution of the ice sheet dynamics simulated in a model, as a function of the representation of different processes and parameter values.

associated uncertainty. Spatial derivatives required by the Taylor series are calculated via a high precision meshless algorithm [47], using a pool of suitable nearby neighbouring observations for both the Taylor series origin and the calculation of the derivatives. An ensemble approach is used to estimate the interpolated value and the uncertainty, with points being drawn randomly from the neighbour pool for both the Taylor series origin and derivative calculation, and robust statistical methods are used to calculate the ensemble central tendency and spread. The method can be applied to both bed topography and texture fields independently.

The above approaches are commonly used in generating bed topographies, including in non-glaciated environments. A key limitation is the neglect of accounting for spatial autocorrelation, which can lead to overly-smoothed or unrealistic bed topographies, particularly in sparsely-sampled regions [40,41]. Furthermore, common interpolation methods are typically used to map gridded bed products onto ice sheet model meshes. Although these interpolation distances are typically much smaller, with correspondingly smaller additional errors and uncertainties than in the generation of the original bed topography, this can introduce a second layer of uncertainties in the meshed bed topographies that can propagate in ice sheet modelling (e.g. see discussion in [2]).

(ii) Linear perturbation theory

Linear perturbation theory has been used to generate bed topographies by deriving transfer functions in Fourier space that link ice surface velocity and elevation to basal properties. For example, building on [48,49], recent studies [50,51] applied steady-state linear perturbation theory and the shallow ice approximation to the full-Stokes equations to generate bed topography datasets for Thwaites and Pine Island Glaciers, West Antarctica. This approach assumes that ice is a linear viscous fluid (i.e. a Newtonian fluid), flowing at a constant speed, and solves the resulting overdetermined system via weighted least squares. The resulting beds realistically capture medium-wavelength features beneath fast-flowing ice, but are associated with higher uncertainty in areas where the shelfy-stream approximation (SSA) to the full-Stokes equations does not hold, such as areas with steep topography. Hence, this method generates bed topographies that aim to realistically capture landforms, and is therefore between the end members (i.e. elevation-preserving or texture-preserving) on the methodological spectrum.

The topography produced by linear perturbation is subject to several uncertainties, including parameters used in the inversion (e.g. mean ice thickness and mean basal slipperiness), limitations in capturing short-wavelength bed features that do not propagate to the surface, and the linearisation approximation (ice is a non-Newtonian fluid). The method divides the domain into discrete regions, solving for topography in each region independently. To estimate uncertainty, the standard deviation of topography in overlapping regions is computed; uncertainties related to the linearisation approximation, and to some extent the inversion parameters, are also quantified.

(iii) Mass conservation

The mass conservation method uses the governing equation for the conservation of mass to reconstruct bed topography in regions of sparse bed measurements [52,53]. Using observed estimates of ice surface velocity and surface mass balance inputs, the mass conservation method solves for ice thickness via the ice flux divergence term ($\nabla \cdot H\bar{\mathbf{v}}$) and ice surface elevation. The method is most suitable in regions of relatively fast flow (i.e. where the ice surface velocity is $\geq$50 m year^{-1}) and where there is a constant ratio of surface to column-averaged velocities (i.e. where SSA applies). Outside these regions, uncertainties in the mass flux term become large, and the method is less reliable.

Mass conservation has been used to generate bed topographies for both the Antarctic and Greenland Ice Sheets. The BedMachine Antarctic and Greenland datasets [52–54] are among the most widely-used topographies in ice sheet modelling applications (e.g. in the Ice Sheet Model Intercomparison Project; [55–59]). To generate these datasets, the mass conservation method was improved to assimilate radar-derived ice thickness estimates [60], such that the resulting bed topographies are close to elevation-preserving.

The uncertainties in BedMachine Antarctica version 3 [53,61] were estimated using a combination of approaches. In fast-flowing regions, uncertainties were estimated by solving a linearised mass conservation equation propagated both downstream and upstream of radar flight lines, taking into account uncertainties in surface velocity and surface mass balance observational estimates. In slow-moving regions, uncertainties are heuristic, with errors assumed to grow linearly as a function of the distance from the nearest measurement, and capped at 1000 m.

An alternative mass conservation approach is TELVIS (Thickness Estimation by a Lagrangian Validated Interpolation Scheme; [62]). TELVIS is a streamline-based mass conservation method that uses ice surface slope and accumulation to infer ice thickness under local mass balance assumptions. This method interpolates along surface streamlines between observations, resulting in low variability along streamlines, but (locally) high variability across flow. To address this issue, Gaussian smoothing is applied to the interpolated topography, such that bed measurements are not necessarily honoured. This method has been used to generate bed topographies in the Aurora Subglacial Basin, East Antarctica. Uncertainties were estimated at each observational point using the TELVIS algorithm in separate computations. That is, for each point, all observational data within a 5 km radius — including the point itself — were excluded from the calculation, and the uncertainty computed as the difference between the TELVIS-predicted ice thickness estimate and the observed value at that point.

(b) Geostatistical methods

Geostatistics comprises stochastic and spatial statistics-based methods to generate bed topography datasets, and associated uncertainties, that are consistent with observed data and known characteristics of the bed, including its texture, roughness or correlation structure [63]. Geostatistical approaches can be categorised into deterministic estimation-based methods (e.g. Kriging), simulation-based methods (e.g. sequential Gaussian simulation, multiple-point direct sampling, Markov chain Monte Carlo), or hybrid/advanced methods (e.g. geostatistical inversion, and combined geostatistical/machine learning approaches).

(i) Kriging

The Kriging family of methods (ordinary, universal, simple, indicator, co-, regression, or Bayesian Kriging) are forms of Gaussian process regression that use spatial covariance information to generate bed estimates at unsampled locations (i.e. Kriging is an elevation-preserving method). Ordinary, universal, and regression Kriging incorporate trends or regression models to integrate the non-stationarity of the data. The objective of Kriging is to optimise local accuracy and interpolate values in such a way that the estimation variance is minimised [64]. An advantage of Kriging is that it produces an estimation variance at each interpolated grid cell, providing a robust uncertainty estimate. Furthermore, although Kriging is mathematically elegant, it can generate "bulls-eye" patterning, whereby systematic, spurious sinks or conical features are introduced into the bed topography. Kriging, by definition, also averages radar bed measurements to perform interpolations, which causes smoothing. As such, Kriging does not reproduce the spatial covariance of observations.

(ii) Geostatistical simulation

While Kriging prioritises interpolation accuracy at the cost of realistic spatial characteristics, geostatistical simulation is designed to reproduce the spatial structure observed in the data [65]. This approach involves generating multiple realisations of bed topography that are conditioned to available measurements and exhibit realistic roughness [63] – i.e. texture-preserving. The resulting ensemble of realisations provides a quantitative measure of uncertainty and enables the propagation of bed uncertainty into downstream models. Geostatistical simulation methods typically fall into two main categories: (1) sequential Gaussian simulation (SGS); and (2) multiple-point statistics (MPS). SGS is the stochastic counterpart to Kriging and is built on the same system of equations. In theory, the mean and variance of an SGS ensemble approximate the Kriging estimate and variance. SGS approaches can account for spatial trends, anisotropy, and even heterogeneous roughness in bed topography [41]. MPS methods, by contrast, are non-parametric and rely on representative training images to model complex spatial patterns [66]. In the context of subglacial topography, MPS uses densely surveyed bed regions and seafloor bathymetry as training data to fill in data gaps [40,67,68]. While MPS excels at simulating complex geological textures, its effectiveness depends critically on the availability, quality, and appropriateness of training images.

(iii) Geostatistical inversion

The advantages of geostatistical simulation and geophysical inversion (e.g. gravity inversion for bathymetry) can be combined through geostatistical inversion [69–72]. Typically, this involves some sort of Markov Chain Monte Carlo (MCMC) approach where geostatistical realisations are iteratively perturbed until forward-modelled synthetic data match the measurements. This framework is advantageous because it allows for the sampling of the parameter space and does not require the inverse problem to be solved directly, making it well-suited for non-unique, non-linear inverse problems. This approach has recently been used to generate bed topography ensembles that are both texture-preserving and consistent with observed fields (i.e. ice surface velocity, elevation and surface mass balance; [73]). The ensemble of topographies generated with

MCMC can be considered as a set of samples from the posterior distribution defined based on the physical constraints. This approach captures the uncertainties associated with different solutions to the same governing equation, such as mass conservation. The ensemble approach enables uncertainties in bed topography to be systematically propagated into ice sheet model simulations.

(c) Machine learning methods

Machine learning, including physics-informed and data-driven approaches, has more recently been used to generate bed topography datasets. As with the approaches outlined above, machine learning models can leverage a range of input data, including ice surface velocity and elevation (and trends), radar observations, and surface mass balance to estimate the underlying bed elevation.

Various machine learning models have been applied to generating bed topography datasets [74–77]. Algorithms such as gradient-boosted decision trees (e.g. XGBoost; [76]) can handle structured data, identifying spatial relationships between features at the surface and the ice-bed interface (i.e. similar to linear perturbation theory). Deep learning models, particularly convolutional neural networks, are designed to identify spatial hierarchies in gridded datasets, and hence resolve features across spatial scales. The performance of a range of machine learning models was assessed in the context of the generation of bed topographies for Greenland [77], with XGBoost providing the best performance.

Although not yet applied in glaciology, other fields such as groundwater hydrology have demonstrated that integrating geostatistical techniques (e.g., universal Kriging), structured data processing, and deep learning can improve the realism of machine learning datasets [78] by enforcing physically-consistent relationships between inputs and predictions. However, the focus on preserving large-scale elevation structure, could also lead to small-scale structures being overly smoothed, highlighting a potential trade-off between physical consistency and high-frequency detail, particularly in sparsely sampled regions.

Uncertainties in bed topographies derived from machine learning models arise from multiple factors, including unevenness in training data coverage (e.g. radar line density), input feature selection, and assumptions in the model architecture. Quantifying these uncertainties is critical, yet often remains ad hoc. Evaluation metrics like RMSE provide a global error estimate, but cannot adequately quantify spatially-variable uncertainty. Ensemble modelling, cross-validation, and uncertainty-aware architectures like Bayesian neural networks are increasingly used to estimate predictive uncertainty [79]; however, standardised approaches for quantifying uncertainty remain limited. Moreover, neural networks often lack clearly defined optimisation goals. In geostatistics, interpolation outcomes are typically explicit: optimising local accuracy (i.e. elevation-preserving, as in Kriging) or spatial variability (i.e. texture-preserving, as in SGS). However, by contrast, neural networks often attempt to satisfy both objectives simultaneously, resulting in outputs that mayb be difficult to interpret.

(d) Joint inversions: disentangling bed topography and basal friction

In the preceding sections, we reviewed approaches to generating synthetic bed topographies through the assimilation of various data streams. The efficacy of some of the approaches outlined above is influenced by underlying assumptions about bed properties, including the basal friction coefficient field and the properties and processes that influence it (figure 1). For example, methods that employ inversion typically assume a fixed spatial structure for the basal friction coefficient, which can lead to unresolved resistance at the bed being attributed to either friction or topography, without the capacity to distinguish between skin drag (frictional resistance) and form drag (arising from bed geometry). This is an issue that has been previously discussed in the literature [10], including in relation to locations where the bed topography is unresolved [80]. It can lead to significant errors in both bed topography and basal friction fields, especially in regions with sparse observations, complex basal processes, or when other ice dynamics processes are poorly constrained [16,81].

An alternative approach is joint inversion (e.g. [82–87]), which simultaneously solves for both the bed topography and basal friction coefficient using surface observables (e.g. velocity and elevation), allowing for a more continuously discretised partitioning between processes that influence basal drag. Such an approach also reduces the risk of compensating errors, including where friction and bed elevation adjust in offsetting ways to fit surface constraints. Ensemble-based Bayesian frameworks (e.g. [82]) also allow quantification of uncertainties and correlations between the inverted fields, helping to identify regions where drag attribution is ambiguous or poorly constrained.

As for all of the methodologies we have reviewed above that require treatment of the basal friction coefficient, joint inversion frameworks typically assume temporally static basal conditions. This limits their ability to represent transient processes in the basal friction field such as evolving subglacial drainage, sediment transport, or other changes associated with grounding line migration. Capturing such processes would require not only joint inversion but also time-dependent data assimilation (e.g. [86]) and more sophisticated treatment of subglacial processes (e.g. [88]). Nevertheless, joint inversion offers a promising pathway to more physically-motivated representations of bed topography and basal friction.

3. Ice sheet sensitivity to bed topography

Understanding the sensitivity of ice sheet evolution to bed topography has been a long-standing focus of ice sheet modelling studies. A common approach to assessing such sensitivity involves generating large ensembles of bed topography realisations, where variations in the bed are informed by uncertainty estimates (e.g. [1,89]) or by adding structured or random noise (e.g. [90,91]), and running prognostic ice sheet model simulations to evaluate differences in the ice sheet response to different bed topography realisations. Such ensemble-based approaches enable quantification of the influence of bed variations on key ice sheet variables. Ensemble approaches can also be used to determine how well the bed must be constrained (i.e. to what level must uncertainty be reduced) to ensure sea-level rise projections remain within a prescribed tolerance. This approach has been recently applied to the Thwaites Glacier catchment [1], where wavelet decomposition was used to construct an ensemble of bed realisations. The study found that to limit global sea level rise uncertainty due to ice loss from Thwaites catchment to ± 2 cm would require constraining bed topography to within 8 m vertically and 2 km horizontally. Note, however, that this resolution requirement may vary spatially.

An alternative approach to assessing ice sheet sensitivity to bed topography is via automatic differentiation [92,93], which quantifies the sensitivity of a model output to perturbations in a given independent input. This method characterises spatial sensitivity, and hence highlights where constraining estimates of an independent variable will be most valuable in constraining propagated uncertainties in the ice sheet evolution. For example, [92] showed that the ice volume above flotation in the Amundsen Sea Sector is largely insensitive to basal friction coefficient variations in the ice sheet interior, but highly sensitive within a few tens of kilometres upstream of the Pine Island and Thwaites Glacier grounding lines. Although automatic differentiation is gaining traction in glaciological applications, it has yet to be applied to assess sensitivities to bed topography.

Ensemble approaches and automatic differentiation provide complementary insights into ice sheet sensitivity. Ensemble approaches assess how uncertainties in bed topography of varying magnitudes and spatial structures influence ice sheet evolution. This is particularly useful for evaluating how errors in elevation or landform (i.e. elevation- versus texture-preserving bed topographies) might affect projections, and for determining the level of observational constraint required in different regions, as discussed above. In contrast, automatic differentiation identifies where the model is most sensitive to perturbations in the bed, independent of their actual magnitude or uncertainty. This makes it a powerful tool for locating regions where small errors

— if present — could have relatively large effects on ice dynamics. The distinction between these two approaches is important when considering physical processes at the ice-bed interface. For example, a region with high form drag may show strong sensitivity to small-scale topographic undulations (e.g. pinning points), which a texture-preserving bed realisation could better capture. Conversely, a region dominated by skin drag might exhibit lower sensitivity to topographic detail but higher sensitivity to friction-related processes. Ensemble methods can capture sensitivity resulting from both, but only automatic differentiation can precisely highlight the mesh point-wise impact of variations on the metric in question (e.g. flux over the grounding line). While our study is based on ensemble methods, future work would benefit from incorporating automatic differentiation to identify the regions and processes that could be targeted for improved realism of ice sheet model projections.

4. Assessing ice sheet sensitivity to bed variations: a case study of the Aurora Subglacial Basin

In this section, we assess the sensitivity of the Aurora Subglacial Basin to bed topography using the Ice-sheet and Sea-level System Model (ISSM; [94]). Aurora Subglacial Basin is one of the most rapidly evolving catchments in East Antarctica [95,96], with ocean-driven ice shelf melt dominating its evolution [3,5,97]. Containing approximately 7 m of equivalent sea level, the Aurora Subglacial Basin has been the subject of several ICECAP (Investigating the Cryospheric Evolution of the Central Antarctic Plateau; [62]) surveys since 2008, resulting in approximately 9.4 million radar points [29] – a coverage of approximately 8.1 points per km^2. However, the data distribution is highly anisotropic, with high along-track point density (median spacing of 12.2 m) while lateral spacing between tracks is typically multiple kilometres. This can lead to relatively large differences between bed topographies generated using the different approaches described above.

Here, we aim to better understand the impacts of the choice of bed topography on simulated sea level rise, and particularly examining where, and to what extent, evolution of the Aurora Subglacial Basin is sensitive to bed topography variations. To this end, we conduct ice sheet model simulations using an ensemble of bed topographies — comprising both elevation- and texture-preserving beds — forced using a high emission scenario to 2300 CE.

(a) Model and approach

(i) Model initialisation

The ice sheet model domain is the IMBIE outline for the Aurora Subglacial Basin, East Antarctica [98], of which the key outlet glaciers are the Vanderford, Totten, and Moscow University Ice Shelf (MUIS) Glaciers (e.g. [99]). The horizontal domain is partitioned into 416,515 triangular elements, with mesh refinement based on the MEaSUREs version 2 ice velocities [100,101], with the horizontal element size increasing from $\sim$500 m near the grounding line to a maximum of 40 km in the interior of the catchment. We use the BedMachine Antarctica version 3 [53] dataset for initial bed and surface elevation, and grounded and floating ice masks to initialise the geometry, reinforcing hydrostatic equilibrium where interpolation errors onto the model mesh lead to floating ice geometry inconsistencies.

Inverse methods [60,102] and the Glen flow law [103–105], in conjunction with the MEaSUREs v2 ice surface velocity fields, are used to determine the ice rigidity on floating ice. We then use the Schoof friction law [106,107] to determine a basal friction coefficient over grounded ice via inversion, again with the MEaSUREs v2 ice surface velocity fields as the observational constraints. To avoid spatial heterogeneities in the basal friction coefficient associated with the neglect of subglacial hydrological processes [88], which are known to be important in this region [18], we follow a similar setup to that described in [20]. Specifically, we generate an effective pressure field from the GlaDS subglacial hydrology model implemented in ISSM (see also [21,22,108]) and use this field as input to the Schoof friction law. More details on the modelling procedure are provided in the supporting text section S1. The resulting effective pressure field and the corresponding friction coefficient calculated using the BedMachine geometries are shown in supporting figure S1, and are temporally invariant for each simulation.

(ii) Control simulation

Starting from the model initial state described above, we perform a 20 year relaxation simulation with a constant ice shelf basal melt rate [109], to ensure model fields are consistent (c.f. [84]). Using the geometries and velocities at the end of the relaxation period, we simulate projections from 2015–2300 CE using the non-local quadratic ISMIP6 melt rate parameterisation [110]. The ocean thermal forcing and surface mass balance fields are derived from the UKESM1-0-LL Shared Socioeconomic Pathway SSP5-8.5 emission scenario, as provided in the ISMIP6 Antarctic 2300 CE forcings [59,111]. We note that this is just one climate forcing scenario, which will impact the consequent timing of onset of grounding line retreat [59]. We choose a high emission scenario so that the spread of results for different bed realisations is greater, noting that the SSP5-8.5 scenario is generally considered to be a high-end, and less likely, scenario. All prognostic simulations of the ice sheet model evolve the momentum and mass balance equations, and grounding line location. A monthly model time step is used, and key model variables are output every model year. The calving front is kept fixed in all simulations.

(iii) Bed topography ensemble

We geostatistically simulate an ensemble of mass-conserving topographic realisations for the Aurora Subglacial Basin using a new Markov chain Monte Carlo approach [73]. This method iteratively perturbs geostatistical realisations of bed topography, using mass conservation as a physical constraint in fast-flowing regions (where surface velocities are $\geq$50 m year^{-1}), until the misfit between simulated and observed velocities is minimised. A total of five ensemble members were generated. To investigate the influence of bed variations distal to the grounding line where ice flow is too low to apply mass conservation constraints, we use a sequential Gaussian simulation (SGS), conditioned on one of the MCMC beds, to generate an additional ten bed realisations (MCMC+SGS). The domain for the MCMC+SGS simulations is shown in figure 2; outside this domain, the bed topography is the BedMachine bed. Using the final geometries and velocities from the relaxation simulation, we run a prognostic simulation for each MCMC and MCMC+SGS bed realisation under the same ocean and atmosphere forcing described in section ii and the same basal friction coefficient as derived for the BedMachine configuration. We then repeat the prognostic simulation, this time using basal friction coefficients generated from inversion for each bed realisation under consideration. The differences in the basal friction coefficient distributions between the BedMachine, MCMC, and MCMC+SGS beds are shown in supporting figure S2, and the Kolmogorov-Smirnov test statistic of significances in the differences between the friction field distributions, along with the corresponding p-values, are shown in supporting table S1.

We conduct separate simulations under the same climate forcing described above, but this time using a bed topography realisation generated using the Stochastic Meshless Uncertainty Gridding (SMUG) algorithm [46], as well as a simulation using the Bedmap3 bed topography [44]. As for the MCMC and MCMC+SGS ensemble above, we run two prognostic simulations for each SMUG and Bedmap3 bed realisation: one with the basal friction coefficient generated using inversion for the BedMachine bed and a separate simulation with the basal friction coefficient generated using inversion for each individual bed realisation.

Figure 2 compares the BedMachine bed with one realisation of each of the MCMC and MCMC+SGS beds, and the SMUG and Bedmap3 beds for a subset of the Aurora Subglacial Basin where the surface speed is $\geq$50 m year^{-1}. A few differences between the bed topographies are worth noting. First, the BedMachine bed is deeper than each of the other bed topographies in the Vanderford Trench within the region ~20–30 km upstream of the present-day Vanderford Glacier grounding line. Second, Bedmap3 is on average deeper than all other bed topographies upstream of the Vanderford Trench, although there are localised regions of higher elevation, and the SMUG and Bedmap3 datasets show the strongest agreement at the small-scale (as might be expected, given both are generated using the same observational data [29]). As expected, the MCMC and MCMC+SGS bed topographies show much larger local deviations from BedMachine than both the SMUG and Bedmap3 bed topographies. The MCMC and MCMC+SGS realisations use the updated Totten bathymetry from [112], which was not incorporated in BedMachine v3.

(b) Sensitivity of ice sheet evolution to ensemble-based projections

The retreat behaviour of the Aurora Subglacial Basin has been well documented in previous studies [3,59,113–115]. Here, we specifically consider the effect of different bed topography and friction coefficient realisations on the timing and rate of grounding line retreat.

Figure 3 shows the rate of change of ice mass above flotation (dM/dt, calculated by converting from ice volume above flotation to ice mass above flotation; left y-axis) and the corresponding global mean sea level equivalent (right y-axis) for each bed realisation. The evolution of both the grounding line location and ice thickness contribute to the change in ice mass above flotation in our simulations; here we focus on describing the pattern in grounding line retreat, which evolves similarly in each simulation.

Glaciers in the Aurora Subglacial Basin show relatively little retreat and mass loss under climate change to approximately 2115 CE (reflected in the smaller dM/dt values in figure 3). From ∼2115–2180 CE, the grounding line retreat accelerates rapidly. This is manifest in the merging of the grounding lines of the Totten, Vanderford, and MUIS Glaciers, and the retreat to the southern edge of the Vanderford Trench, which is a topographic barrier to the inland Aurora Subglacial Basin. Ice mass loss continues beyond 2180 CE, with an increasing spread in the sea level rise estimates, i.e. reflecting sensitivity to the bed topography and friction coefficient realisation.

We observe a systematic difference in the magnitude of dM/dt and the sea level equivalent between the Bedmachine, SMUG, and Bedmap3 topographies and the MCMC ensembles (figure 3). In particular, the BedMachine, SMUG, and Bedmap3 simulations generally reflect the greatest absolute rate of mass loss over the period of marked grounding line acceleration from 2115–2180 CE, and the largest sea level rise by 2300 CE. By contrast, the MCMC ensembles — both MCMC and MCMC+SGS and for all friction coefficient realisations — have the lowest mass loss to 2300 CE. Given that the simulations start from a different initial ice volume (due to differences in the bed topography and hence ice thickness; although the maximum difference in initial ice mass above flotation is 0.36%), it is not unexpected that the initial dM/dt values vary accordingly. However, despite these variations in dM/dt magnitude, the overall shape of dM/dt for all simulations is very similar, which highlights the importance of the large horizontal-scale bed variations in determining the overall behaviour in the grounding line evolution of this region.

As expected, the dM/dt and sea level contributions reflect differences in both the bed topographies and the basal friction coefficients. Generally, the simulations that use the same friction coefficient as BedMachine show a much larger spread, equating to a greater systematic difference in final sea level contributions (∼23% difference between largest and smallest sea level equivalent from all ensemble members) than the simulations with friction coefficients optimised for each bed realisation (∼11% difference between largest and smallest sea level equivalent). Interestingly, the difference between sea level contributions in the MCMC members that use the two different friction coefficient approaches are generally larger than the spread between individual members of each set. Supporting figure S2 shows the differences in friction coefficient distributions for each bed realisation. We note that the differences in the distributions of friction coefficients are not statistically significantly different between any ensemble member compared with the BedMachine friction coefficient. Instead, small-scale variations in the friction coefficient in the region close to the grounding line lead to these markedly different results.

Next, we examine the differences in the evolution of the grounding line location as a function of variations in bed topography and basal friction coefficient. Figure 4 shows the grounding line evolution along six streamlines calculated using the MEaSUREs v2 ice surface velocity fields, focussed on the Totten and MUIS Glaciers. For simplicity, in figure 4 we show only the results that use the the same friction coefficient realisation (derived from inversion using the BedMachine bed), comparing results for BedMachine, SMUG, Bedmap3, and one MCMC realisation. The full set of comparisons are shown in supporting figure S3. All beds generally capture the same large horizontal-scale variations, with greater vertical differences at finer horizontal scales. This is particularly notable for profiles 3 and 4, where local vertical differences between the BedMachine and MCMC beds can be greater than 200 m across horizontal scales of 2-5 km. Large vertical differences in the bed do not necessarily always translate to large differences in the evolution of the grounding line retreat except where they influence: (1) the timing of the onset of grounding line retreat; and (2) the final grounding line position. For example, there is relatively little difference in the grounding line evolution of profiles 1 and 2: grounding line retreat initiates at a similar year, the rate of retreat is very consistent between different ensemble members, and the final grounding line position is very similar. For profile 3, the BedMachine, SMUG, and Bedmap3 grounding line retreat is delayed by 50-100 years compared with the MCMC ensemble; once initiated, grounding line retreat occurs very similarly for all bed topographies. For profile 4, again, the grounding line retreat rate is similar across simulations, except in the final $\sim$100 years, where the BedMachine, SMUG, and Bedmap3 simulations show $\sim$25 km more grounding line retreat than the MCMC ensemble, most likely linked to larger systematic differences between these bed elevation realisations compared with the MCMC ensemble members. For profiles 5 and 6, the timing of the onset of retreat and the final grounding line positions vary more considerably, again as a function of variations in the bed, with the MCMC bed showing earlier retreat onset. As expected (given the dM/dt and sea level results in figure 3), the differences across the MCMC and MCMC+SGS ensemble members are generally smaller than the differences between the MCMC and MCMC+SGS ensembles and the BedMachine, SMUG and Bedmap3 realisations (figure S3).

5. Discussion

We first revisit the utility of synthetic bed topographies in light of their underlying design objectives: namely, whether they preserve elevation or texture. As discussed in section 2, elevation-preserving datasets aim to realistically represent the large-scale shape and gradients in the bed, and therefore might produce a more realistic response in ice sheet models where the data density is sufficiently high to constrain key bed features. However, the key question here is what is dense enough? A previous study [1] demonstrated that, to constrain sea level rise uncertainty within $\pm$20 cm from Thwaites Glacier, bed observations must be spaced at least every 2 km horizontally, with a vertical accuracy of at least 8 m. No such density in radar surveys exists at the catchment-scale, particularly within critical regions likely to contribute to sea level rise over the coming centuries [58,59]. Ensemble approaches based on elevation-preserving bed topographies (e.g. [1,89]) can provide insight into the effects of the bed uncertainty on the ice sheet evolution, but the representativeness of simulated landform amplitude and wavelength — and the ability of such datasets to capture the character of pinning points — remains a central challenge.

In contrast, texture-preserving topographies, such as the MCMC and MCMC+SGS realisations examined here, aim to reproduce the statistical structure of surveyed landforms, including the amplitude and periodicity of bed undulations observed in radar data. These datasets are designed to replicate the morphology of landforms, such as subglacial ridges, troughs, and rough patches, even where observations are sparse. By preserving textural properties, they may offer an improved representation of the characteristics of likely pinning points and other features, specific to the region of interest, and which are crucial for simulations of grounding line retreat. While such datasets may sacrifice small-scale elevation accuracy, their ability to realistically sample the range of bed geometries expected in Antarctic catchments is valuable for robust uncertainty quantification in ice sheet models, particularly in regions where data are sparse. Ultimately, texture-preserving topographies can complement elevation-preserving approaches by capturing unsampled fine-scale bed features that may strongly control ice dynamics.

A key element of all the bed datasets discussed in this study is their estimate of uncertainty. Robust uncertainty estimates of bed topography are critical because they define the limits of what can be inferred, both about a given bed topography dataset and the ice sheet model experimental design. Uncertainties comprise observational, intra- and inter-algorithm differences, and the method of interpolation onto ice sheet model grids (which is a function of the model resolution), and can directly influence ice sheet dynamics, including through parameters like the basal friction coefficient. Furthermore, when uncertainties are robustly quantified, they can be used in ice sheet model simulations (including e.g. through analyses such as the DAKOTA framework [32,33]), and the results can be used to inform experimental design, model sensitivity studies, and future airborne radar surveys targeting observations of the ice-bed interface.

In section 5(a) below, we discuss implications of our case study focused on how different bed topographies, including both elevation- and texture-preserving beds, impact ice sheet evolution and associated sea level contributions from the Aurora Subglacial Basin, East Antarctica. While this provides important insight into one key impact of bed uncertainties — i.e. sea level rise — bed topography also influences other processes at the ice-bed interface, including heat transfer, which impact the basal ice temperature, basal melt rates, sliding, and subglacial hydrology. We discuss these in more detail in section 5(b).

(a) Ice sheet sensitivity to bed topography in the Aurora Subglacial Basin

A key aim of our study was to investigate ice sheet sensitivity to bed variations. We did this using an ensemble ice sheet modelling approach with different realisations of bed topography.

Overall, we find that small differences in the bed topography (and friction coefficient, as discussed in more detail in section 5(b) below) can significantly impact ice sheet evolution in the Aurora Subglacial Basin. In particular, the timing of the onset of grounding line retreat locally varies by up to $\sim$100 years depending on the bed topography realisation, with some simulations showing immediate retreat from the start of the forcing period. We highlight *local* here, given that while all bed realisations similarly captured the large-scale bed features of the region, it was local differences in key regions — close to the present-day grounding line and the upstream edge of the Vanderford Trench — that led to the marked differences in the timing of the onset of retreat and final grounding line position (e.g. [2,4]). This highlights the urgent need for targeted radar surveys to constrain the bed topography directly upstream of the present-day grounding line, and within the region of likely grounding line retreat over the coming decades to centuries.

Despite local vertical differences in bed topography realisations of over 200 m, the rate of retreat, once initiated, was relatively insensitive to the bed elevation. That is, all our simulations showed very consistent retreat rates for both optimised and non-optimised friction coefficients [116]. This could be partly related to particulars of this system. That is, the retreat of the Totten and Vanderford Glaciers through the deeply-incised Vanderford Trench and between the eastern flank of the Totten and MUIS Glaciers, is rapid once initiated, a finding that is also supported by the inferred geomorphology of the basin [113]. This behaviour is consistent with the region's marine-based bed and vulnerability to a warming ocean.

Given that we did not use automatic differentiation in this study, we cannot say from our experiments where the system is most sensitive to uncertainties in the bed topography – i.e. how the magnitude versus the location of bed variations impact the system. Nevertheless, given that the MCMC beds vary from the BedMachine bed topography only within the 50–100 km upstream of the present-day grounding line, our simulations reflect high sensitivity to bed topography near the grounding line, which is consistent with previous studies (e.g. [1,89]). Interestingly, the MCMC+SGS simulations (although all conditioned on one realisation of MCMC) show consistently less sea level contributions than any of the MCMC simulations, which is evidence that distal bed topography can influence ice mass loss; however, this effect is secondary compared with the effects of differences close to the grounding line.

Finally, we observed a systematic difference in sea level projections derived from the elevation- and texture-preserving bed realisations analysed here. The SMUG, Bedmap3, and MCMC datasets were all generated using the same underlying input data (i.e., [29]). Although BedMachine v3 does not include the updates from [29], the limited additional data from new surveys in the Aurora Subglacial Basin is unlikely to substantially change the BedMachine bed topography for this region. Furthermore, the differences between the BedMachine and MCMC beds are not systematically larger than the differences between either the Bedmap3 or SMUG beds and the MCMC beds, which strengthens our confidence that the systematic differences in the MCMC-derived sea level estimates are not due to discrepancies in input bed topography data. Rather, the differences may stem from differences in the structural and statistical approaches used to generate the MCMC ensemble compared with the other datasets, including e.g. the "roughness" of the MCMC beds compared with the other beds and the effect of the texture on the simulated buttressing. The relatively small size of the MCMC bed ensemble means it may not fully capture the broader uncertainty space associated with that method, and further bed realisations may be needed to assess whether the observed differences are representative or a result of a too-small sample size. Our preliminary findings suggest that methodological choices — such as how bed topography variability and uncertainty are represented, even if the differences are localised — can have a significant impact on derived sea level estimates. This highlights the importance of using bed ensembles and how the design objectives for generating bed topographies may influence the kinds of questions they can be used to address.

(b) Looking forward: constraining properties and processes at the ice-bed interface

In this study, we focused on the sensitivity of projected sea level rise to variations in bed topography and friction coefficient. When the basal friction coefficient was optimised individually for each bed topography, differences in projected SLR to 2300 CE were smaller (maximum difference of 11%). However, a larger spread (up to 23%) emerged when a constant friction coefficient was imposed across all ensemble members, with particularly divergent sea level contributions over time. This result is expected, given that the non-optimised basal friction fields were inconsistent with all but the BedMachine ice sheet initial state (e.g. geometry, velocities), which can shock the system into a more rapid onset of retreat. That is, the power of data assimilation approaches, like the inverse method employed here, is that they optimise the friction coefficient for the particular model fields – the surface velocity and ice geometry – and hence better capture the ice sheet state at a snapshot in time [102]. Recent developments have incorporated transient data assimilation so that trends (e.g. in ice thickness) are also accurately represented [117] on decadal timescales. However, inverse methods achieve that at the potential risk of overfitting [118,119], such that relatively small differences in the friction coefficient arising from inconsistencies between input fields can lead to relatively large differences in sea level rise, as we found here. Indeed, the median of the maximum percentage difference between the BedMachine friction coefficient and each of the 17 other optimised friction coefficient fields is 1.34% (minimum 0.95%; maximum 8.09%). The effects of this, and of prescribing temporally constant basal friction coefficients, on the long-term evolution of the ice sheet remain an open question. It follows that understanding the processes that influence basal friction and how they are represented in ice sheet models is essential for developing physically-informed parameterisations that complement and strengthen data assimilation approaches. Here we discuss a number of properties and processes at the ice-bed interface that are relevant to consider in improving the representation of basal friction.

Basal friction is influenced by several related factors, including the: (1) bed topography, which influences form drag directly as ice flows over topography, and skin drag indirectly through modulation of the subglacial hydrology and local frictional forces (e.g. [10]); (2) geological substrate, that influences the relative contributions of hard-bedded sliding versus bed deformation [106,120,121]; (3) subglacial hydrology, particularly the presence of an inefficient/distributed drainage system, which strongly controls the effective pressure at the bed [18–20]; and (4) heat sources at the bed, including geothermal, frictional, and deformational heating, which together influence basal meltwater production [122], and the temperature, and hence viscosity, of the basal ice [17]. The above factors are strongly interdependent and are modulated by the bed topography, through its influence on drag, and both frictional and deformational heat production at the ice base. For example, bed roughness can lead to the formation of basal temperate layers through increases in local shear deformation relative to a smoother realisation of the bed, with implications for the balance between ice flow processes [14]. Topography further affects the direction and concentration of geothermal heat flow to the basal ice layers: depending on the shape and thermal conductivity of the subglacial material, geothermal heat can funnel heat into valleys and depressions where thermal gradients and conductivity are highest or to ridges where the ice has lower thermal conductivity [28,123].

Topography and the permeability of the bed substrate also control the nature of the subglacial hydrological system. Rough topography promotes variable water flow pathways [41], influencing basal sliding and the redistribution of heat by basal water [124]. Topographic depressions can act as thermal water reservoirs, where latent heat exchange through freeze-melt cycles regulate basal temperatures [125]. The geological substrate also influences whether efficient or inefficient drainage systems are supported, which in turn shapes the basal friction and flow regime, and the relative contributions of sliding versus deformational flow [16].

These coupled processes feedback into sea level projections via their influence on grounding line dynamics. Several ice sheet modelling studies have investigated the effects of some of these feedbacks (including e.g. [21,22]), and some ice sheet models explicitly parameterise processes in the till (e.g. [126]). However, work still remains to better understand interactions between the ice thermo-mechanical, subglacial hydrological, and geological systems, the timescales over which they are relevant, and how they can be better represented in ice sheet models.

6. Conclusion

This study examined the utility of bed topographies generated with different objectives — namely elevation- versus texture-preserving beds — and corresponding differences in basal friction coefficients, on ice sheet model simulations of sea level rise in the Aurora Subglacial Basin, East Antarctica. While we identified systematic differences between the sea levels predicted using bed realisations generated to preserve elevation versus texture, the relatively small size of the MCMC ensemble limits our ability to determine whether this finding is robust. Expanding the MCMC ensemble will be needed to fully characterise the uncertainty and understand the implications of these differing objectives. Our results point to the importance of constraining bed topography datasets, and the value of targeted surveys focused on regions directly upstream of marine grounding lines, where bed uncertainty has the greatest impact on ice sheet-driven sea level rise. Finally, our simulations highlight the critical role of the basal friction coefficient in shaping ice sheet evolution, whereby small, localised variations in the basal friction field can lead to large differences in the timing of grounding line retreat and ultimate sea level contributions. Given that the basal friction fields we generated were optimised for ice sheet geometry at a particular snapshot in time, this has implications for the applicability of such fields for long-term ice sheet projections. We advocate for the development of process-based representations of basal friction for ice sheet modelling, which capture relevant ice-bed properties and transient processes realistically and ideally at low computational cost.

Acknowledgements. This research was supported by the Australian Research Council (ARC) Special Research Initiative (SRI) Securing Antarctica's Environmental Future (SR200100005), the ARC Discovery Early Career Award (DE210101433), ARC Discovery Project (DP190100418), the ARC Special Research Initiative Australian Centre for Excellence in Antarctic Science (SR200100008), and in part by grant NSF PHY-2309135 to the Kavli Institute for Theoretical Physics (KITP). CD was supported by the Natural Sciences and Engineering Research Council of Canada (NSERC RGPIN-03761-2017) and the Canada Research Chairs Program (CRC 950-231237). This paper is a contribution to Australian Antarctic Science projects 4077, 4346 and 4511.

References

1. Castleman BA, Schlegel NJ, Caron L, Larour E, Khazendar A. 2022 Derivation of Bedrock Topography Measurement Requirements for the Reduction of Uncertainty in Ice-Sheet Model Projections of Thwaites Glacier. *The Cryosphere* **16**, 761–778. (10.5194/tc-16-761-2022)
2. Houriez L, Larour E, Caron L, Schlegel NJ, Adhikari S, Ivins E, Pelle T, Seroussi H, Darve E, Fischer M. 2025 Capturing Solid Earth and Ice Sheet Interactions: Insights from Reinforced Ridges in Thwaites Glacier. (10.5194/egusphere-2024-4136)
3. McCormack FS, Roberts JL, Gwyther DE, Morlighem M, Pelle T, Galton-Fenzi BK. 2021 The Impact of Variable Ocean Temperatures on Totten Glacier Stability and Discharge. *Geophysical Research Letters* **48**, e2020GL091790. (10.1029/2020GL091790)
4. Robel AA, Pegler SS, Catania G, Felikson D, Simkins LM. 2022 Ambiguous stability of glaciers at bed peaks. *Journal of Glaciology* **68**, 1177–1184. (10.1017/jog.2022.31)
5. Roberts JL, Galton-Fenzi BK, Paolo FS, Donnelly C, Gwyther DE, Padman L, Young D, Warner R, Greenbaum J, Fricker HA, Payne AJ, Cornford S, Le Brocq A, van Ommen T, Blankenship D, Siegert MJ. 2017 Ocean Forced Variability of Totten Glacier Mass Loss. *Geological Society, London, Special Publications* **461**. (10.1144/SP461.6)
6. Schoof C. 2007 Marine Ice-Sheet Dynamics. Part 1. The Case of Rapid Sliding. *Journal of Fluid Mechanics* **573**, 27–55. (10.1017/S0022112006003570)
7. Schoof C. 2012 Marine Ice Sheet Stability. *Journal of Fluid Mechanics* **698**, 62–72. (10.1017/jfm.2012.43)
8. Sergienko OV, Wingham DJ. 2022 Bed Topography and Marine Ice-Sheet Stability. *Journal of Glaciology* **68**, 124–138. (10.1017/jog.2021.79)
9. Weertman J. 1974 Stability of the Junction of an Ice Sheet and an Ice Shelf. *Journal of Glaciology* **13(67)**, 3–11.
10. Kyrke-Smith TM, Gudmundsson GH, Farrell PE. 2018 Relevance of Detail in Basal Topography for Basal Slipperiness Inversions: A Case Study on Pine Island Glacier, Antarctica. *Frontiers in Earth Science* **6**. (10.3389/feart.2018.00033)
11. Matsuoka K, Hindmarsh RCA, Moholdt G, Bentley MJ, Pritchard HD, Brown J, Conway H, Drews R, Durand G, Goldberg D, Hattermann T, Kingslake J, Lenaerts JTM, Martín C, Mulvaney R, Nicholls KW, Pattyn F, Ross N, Scambos T, Whitehouse PL. 2015 Antarctic Ice Rises and Rumples: Their Properties and Significance for Ice-Sheet Dynamics and Evolution. *Earth-Science Reviews* **150**, 724–745. (10.1016/j.earscirev.2015.09.004)
12. Gudmundsson GH, Paolo FS, Adusumilli S, Fricker HA. 2019 Instantaneous Antarctic Ice Sheet Mass Loss Driven by Thinning Ice Shelves. *Geophysical Research Letters* **46**, 13903–13909. (10.1029/2019GL085027)
13. Reese R, Gudmundsson GH, Levermann A, Winkelmann R. 2018 The Far Reach of Ice-Shelf Thinning in Antarctica. *Nature Climate Change* **8**, 53–57. (10.1038/s41558-017-0020-x)
14. Law R, Christoffersen P, MacKie E, Cook S, Haseloff M, Gagliardini O. 2023 Complex Motion of Greenland Ice Sheet Outlet Glaciers with Basal Temperate Ice. *Science Advances* **9**, eabq5180. (10.1126/sciadv.abq5180)
15. Law R, Chandler D, Born A. 2025 What Is Glacier Sliding. (10.48550/arXiv.2407.13577)
16. McCormack FS, Warner RC, Seroussi H, Dow CF, Roberts JL, Treverrow A. 2022 Modeling the Deformation Regime of Thwaites Glacier, West Antarctica, Using a Simple Flow Relation for Ice Anisotropy (ESTAR). *Journal of Geophysical Research: Earth Surface* **127**, e2021JF006332. (10.1029/2021JF006332)
17. Pattyn F. 2010 Antarctic Subglacial Conditions Inferred from a Hybrid Ice Sheet/Ice Stream Model. *Earth and Planetary Science Letters* **295**, 451–461. (10.1016/j.epsl.2010.04.025)
18. Dow CF, McCormack FS, Young DA, Greenbaum JS, Roberts JL, Blankenship DD. 2020 Totten Glacier Subglacial Hydrology Determined from Geophysics and Modeling. *Earth and Planetary Science Letters* **531**, 115961. (10.1016/j.epsl.2019.115961)
19. Dow CF, Ross N, Jeofry H, Siu K, Siegert MJ. 2022 Antarctic Basal Environment Shaped by High-Pressure Flow through a Subglacial River System. *Nature Geoscience* **15**, 892–898. (10.1038/s41561-022-01059-1)
20. Ehrenfeucht S, Dow C, McArthur K, Morlighem M, McCormack FS. 2025 Antarctic Wide Subglacial Hydrology Modeling. *Geophysical Research Letters* **52**, e2024GL111386. (10.1029/2024GL111386)
21. Pelle T, Greenbaum JS, Dow CF, Jenkins A, Morlighem M. 2023 Subglacial Discharge

Accelerates Future Retreat of Denman and Scott Glaciers, East Antarctica. *Science Advances* **9**, eadi9014. (10.1126/sciadv.adi9014)

22. Pelle T, Greenbaum JS, Ehrenfeucht S, Dow CF, McCormack FS. 2024 Subglacial Discharge Accelerates Dynamic Retreat of Aurora Subglacial Basin Outlet Glaciers, East Antarctica, Over the 21st Century. *Journal of Geophysical Research: Earth Surface* **129**, e2023JF007513. (10.1029/2023JF007513)
23. Galton-Fenzi B, Maraldi C, Coleman R, Hunter J. 2008 The Cavity under the Amery Ice Shelf, East Antarctica. *Journal of Glaciology* **54**, 881–887. (10.3189/002214308787779898)
24. Greenbaum JS, Blankenship DD, Young DA, Richter TG, Roberts JL, Aitken ARA, Legresy B, Schroeder DM, Warner RC, van Ommen TD, Siegert MJ. 2015 Ocean Access to a Cavity beneath Totten Glacier in East Antarctica. *Nature Geoscience* **8**, 294–298. (10.1038/ngeo2388)
25. Goldberg DN, Smith TA, Narayanan SHK, Heimbach P, Morlighem M. 2020 Bathymetric Influences on Antarctic Ice-Shelf Melt Rates. *Journal of Geophysical Research: Oceans* **125**, e2020JC016370. (10.1029/2020JC016370)
26. Haigh M, Holland PR, Jenkins A. 2023 The Influence of Bathymetry Over Heat Transport Onto the Amundsen Sea Continental Shelf. *Journal of Geophysical Research: Oceans* **128**, e2022JC019460. (10.1029/2022JC019460)
27. Colgan W, MacGregor JA, Mankoff KD, Haagenson R, Rajaram H, Martos YM, Morlighem M, Fahnestock MA, Kjeldsen KK. 2021 Topographic Correction of Geothermal Heat Flux in Greenland and Antarctica. *Journal of Geophysical Research: Earth Surface* **126**, e2020JF005598. (10.1029/2020JF005598)
28. Willcocks S, Hasterok D, Jennings S. 2021 Thermal Refraction: Implications for Subglacial Heat Flux. *Journal of Glaciology* **67**, 875–884. (10.1017/jog.2021.38)
29. Frémand AC, Fretwell P, Bodart JA, Pritchard HD, Aitken A, Bamber JL, Bell R, Bianchi C, Bingham RG, Blankenship DD, Casassa G, Catania G, Christianson K, Conway H, Corr HFJ, Cui X, Damaske D, Damm V, Drews R, Eagles G, Eisen O, Eisermann H, Ferraccioli F, Field E, Forsberg R, Franke S, Fujita S, Gim Y, Goel V, Gogineni SP, Greenbaum J, Hills B, Hindmarsh RCA, Hoffman AO, Holmlund P, Holschuh N, Holt JW, Horlings AN, Humbert A, Jacobel RW, Jansen D, Jenkins A, Jokat W, Jordan T, King E, Kohler J, Krabill W, Kusk Gillespie M, Langley K, Lee J, Leitchenkov G, Leuschen C, Luyendyk B, MacGregor J, MacKie E, Matsuoka K, Morlighem M, Mouginot J, Nitsche FO, Nogi Y, Nost OA, Paden J, Pattyn F, Popov SV, Rignot E, Rippin DM, Rivera A, Roberts J, Ross N, Ruppel A, Schroeder DM, Siegert MJ, Smith AM, Steinhage D, Studinger M, Sun B, Tabacco I, Tinto K, Urbini S, Vaughan D, Welch BC, Wilson DS, Young DA, Zirizzotti A. 2023 Antarctic Bedmap Data: Findable, Accessible, Interoperable, and Reusable (FAIR) Sharing of 60 Years of Ice Bed, Surface, and Thickness Data. *Earth System Science Data* **15**, 2695–2710. (10.5194/essd-15-2695-2023)
30. Clyne ER, Anandakrishnan S, Muto A, Alley RB, Voigt DE. 2020 Interpretation of Topography and Bed Properties beneath Thwaites Glacier, West Antarctica Using Seismic Reflection Methods. *Earth and Planetary Science Letters* **550**, 116543. (10.1016/j.epsl.2020.116543)
31. Tsutaki S, Fujita S, Kawamura K, Abe-Ouchi A, Fukui K, Motoyama H, Hoshina Y, Nakazawa F, Obase T, Ohno H, Oyabu I, Saito F, Sugiura K, Suzuki T. 2022 High-Resolution Subglacial Topography around Dome Fuji, Antarctica, Based on Ground-Based Radar Surveys over 30 Years. *The Cryosphere* **16**, 2967–2983. (10.5194/tc-16-2967-2022)
32. Larour E, Schiermeier J, Rignot E, Seroussi H, Morlighem M, Paden J. 2012 Sensitivity Analysis of Pine Island Glacier Ice Flow Using ISSM and DAKOTA. *Journal of Geophysical Research-space Physics* **117, F02009**, 1–16. (10.1029/2011JF002146)
33. Schlegel NJ, Seroussi H, Schodlok MP, Larour EY, Boening C, Limonadi D, Watkins MM, Morlighem M, van den Broeke MR. 2018 Exploration of Antarctic Ice Sheet 100-Year Contribution to Sea Level Rise and Associated Model Uncertainties Using the ISSM Framework. *The Cryosphere* **12**, 3511–3534. (10.5194/tc-12-3511-2018)
34. Seroussi H, Morlighem M, Rignot E, Larour E, Aubry D, Ben Dhia H, Kristensen SS. 2011 Ice Flux Divergence Anomalies on 79north Glacier, Greenland. *Geophysical Research Letters* **38**, 1–5.
35. Dorschel B, Hehemann L, Viquerat S, Warnke F, Dreutter S, Tenberge YS, Accettella D, An L, Barrios F, Bazhenova E, Black J, Bohoyo F, Davey C, De Santis L, Dotti CE, Fremand AC, Fretwell PT, Gales JA, Gao J, Gasperini L, Greenbaum JS, Jencks JH, Hogan K, Hong JK, Jakobsson M, Jensen L, Kool J, Larin S, Larter RD, Leitchenkov G, Loubrieu B, Mackay K, Mayer L, Millan R, Morlighem M, Navidad F, Nitsche FO, Nogi Y, Pertuisot C, Post AL,

Pritchard HD, Purser A, Rebesco M, Rignot E, Roberts JL, Rovere M, Ryzhov I, Sauli C, Schmitt T, Silvano A, Smith J, Snaith H, Tate AJ, Tinto K, Vandenbossche P, Weatherall P, Wintersteller P, Yang C, Zhang T, Arndt JE. 2022 The International Bathymetric Chart of the Southern Ocean Version 2. *Scientific Data* **9**, 275. (10.1038/s41597-022-01366-7)

36. Bird LA, Ogarko V, Ailleres L, Grose L, Giraud J, McCormack FS, Gwyther DE, Roberts JL, Jones RS, Mackintosh AN. 2025 Gravity-Derived Antarctic Bathymetry Using the Tomofast-x Open-Source Code: A Case Study of Vincennes Bay. *EGUsphere* pp. 1–38. (10.5194/egusphere-2025-211)
37. Charrassin R, Millan R, Rignot E, Scheinert M. 2025 Bathymetry of the Antarctic Continental Shelf and Ice Shelf Cavities from Circumpolar Gravity Anomalies and Other Data. *Scientific Reports* **15**, 1214. (10.1038/s41598-024-81599-1)
38. Scheinert M, Ferraccioli F, Schwabe J, Bell R, Studinger M, Damaske D, Jokat W, Aleshkova N, Jordan T, Leitchenkov G, Blankenship DD, Damiani TM, Young D, Cochran JR, Richter TD. 2016 New Antarctic Gravity Anomaly Grid for Enhanced Geodetic and Geophysical Studies in Antarctica. *Geophysical Research Letters* **43**, 600–610. (10.1002/2015GL067439)
39. Scheinert M, Zingerle P, Schaller T, Pail R, Willberg M. 2021 Towards an Updated, Enhanced Regional Gravity Field Solution for Antarctica. In *EGU General Assembly Conference Abstracts* pp. EGU21–9873. (10.5194/egusphere-egu21-9873)
40. MacKie EJ, Schroeder DM. 2020 Geostatistically Simulating Subglacial Topography with Synthetic Training Data. In *IGARSS 2020 - 2020 IEEE International Geoscience and Remote Sensing Symposium* pp. 2991–2994. (10.1109/IGARSS39084.2020.9324563)
41. MacKie EJ, Field M, Wang L, Yin Z, Schoedl N, Hibbs M, Zhang A. 2023 GMD - GStatSim V1.0: A Python Package for Geostatistical Interpolation and Conditional Simulation. *Geoscientific Model Development* **16**, 3765–3783. (10.5194/gmd-16-3765-2023)
42. Lythe M, Vaughan DG. 2001 BEDMAP: A New Ice Thickness and Subglacial Topographic Model of Antarctica.. *Journal of Geophysical Research-space Physics* **106 (B6)**, 11,335–11,351.
43. Fretwell P, Pritchard HD, Vaughan DG, Bamber JL, Barrand NE, Bell R, Bianchi C, Bingham RG, Blankenship DD, Casassa G, Catania G, Callens D, Conway H, Cook AJ, Corr HFJ, Damaske D, Damm V, Ferraccioli F, Forsberg R, Fujita S, Gim Y, Gogineni P, Griggs JA, Hindmarsh RCA, Holmlund P, Holt JW, Jacobel RW, Jenkins A, Jokat W, Jordan T, King EC, Kohler J, Krabill W, Riger-Kusk M, Langley KA, Leitchenkov G, Leuschen C, Luyendyk BP, Matsuoka K, Mouginot J, Nitsche FO, Nogi Y, Nost OA, Popov SV, Rignot E, Rippin DM, Rivera A, Roberts J, Ross N, Siegert MJ, Smith AM, Steinhage D, Studinger M, Sun B, Tinto BK, Welch BC, Wilson D, Young DA, Xiangbin C, Zirizzotti A. 2013 Bedmap2: Improved Ice Bed, Surface and Thickness Datasets for Antarctica. *The Cryosphere* **7**, 375–393. (10.5194/tc-7-375-2013)
44. Pritchard HD, Fretwell PT, Fremand AC, Bodart JA, Kirkham JD, Aitken A, Bamber J, Bell R, Bianchi C, Bingham RG, Blankenship DD, Casassa G, Christianson K, Conway H, Corr HFJ, Cui X, Damaske D, Damm V, Dorschel B, Drews R, Eagles G, Eisen O, Eisermann H, Ferraccioli F, Field E, Forsberg R, Franke S, Goel V, Gogineni SP, Greenbaum J, Hills B, Hindmarsh RCA, Hoffman AO, Holschuh N, Holt JW, Humbert A, Jacobel RW, Jansen D, Jenkins A, Jokat W, Jong L, Jordan TA, King EC, Kohler J, Krabill W, Maton J, Gillespie MK, Langley K, Lee J, Leitchenkov G, Leuschen C, Luyendyk B, MacGregor JA, MacKie E, Moholdt G, Matsuoka K, Morlighem M, Mouginot J, Nitsche FO, Nost OA, Paden J, Pattyn F, Popov S, Rignot E, Rippin DM, Rivera A, Roberts JL, Ross N, Ruppel A, Schroeder DM, Siegert MJ, Smith AM, Steinhage D, Studinger M, Sun B, Tabacco I, Tinto KJ, Urbini S, Vaughan DG, Wilson DS, Young DA, Zirizzotti A. 2025 Bedmap3 Updated Ice Bed, Surface and Thickness Gridded Datasets for Antarctica. *Scientific Data* **12**, 414. (10.1038/s41597-025-04672-y)
45. Hutchinson MF. 1989 A New Procedure for Gridding Elevation and Stream Line Data with Automatic Removal of Spurious Pits. *Journal of Hydrology* **106**, 211–232. (10.1016/0022-1694(89)90073-5)
46. Jong LM, Roberts JL, McCormack FS, Fabela Hinojosa A. 2025 Antarctic bed topography estimation using a Stochastic Meshless Uncertainty Gridding (SMUG) method. Manuscript in preparation.
47. Roberts JL. 2024 Meshless weighting coefficients for arbitrary nodes: The efficient computation to machine precision using hyper-dual numbers. *Advances in Engineering Software* **197**, 103753. (10.1016/j.advengsoft.2024.103753)
48. Budd WF. 1970 Ice Flow Over Bedrock Perturbations. *Journal of Glaciology* **9**, 29–48.

(10.3189/S0022143000026770)

49. Gudmundsson GH. 2003 Transmission of Basal Variability to a Glacier Surface. *Journal of Geophysical Research: Solid Earth* **108**. (10.1029/2002JB002107)
50. Ockenden H, Bingham RG, Curtis A, Goldberg D. 2022 Inverting Ice Surface Elevation and Velocity for Bed Topography and Slipperiness beneath Thwaites Glacier. *The Cryosphere* **16**, 3867–3887. (10.5194/tc-16-3867-2022)
51. Ockenden H, Bingham RG, Curtis A, Goldberg D. 2023 Ice-Flow Perturbation Analysis: A Method to Estimate Ice-Sheet Bed Topography and Conditions from Surface Datasets. *Journal of Glaciology* **69**, 1677–1686. (10.1017/jog.2023.50)
52. Morlighem M, Williams CN, Rignot E, An L, Arndt JE, Bamber JL, Catania G, Chauché N, Dowdeswell JA, Dorschel B, Fenty I, Hogan K, Howat I, Hubbard A, Jakobsson M, Jordan TM, Kjeldsen KK, Millan R, Mayer L, Mouginot J, Noël BPY, O'Cofaigh C, Palmer S, Rysgaard S, Seroussi H, Siegert MJ, Slabon P, Straneo F, van den Broeke MR, Weinrebe W, Wood M, Zinglersen KB. 2017 BedMachine v3: Complete Bed Topography and Ocean Bathymetry Mapping of Greenland from Multi-Beam Echo Sounding Combined with Mass Conservation. *Geophys. Res. Lett.* **44**, 11,051–11,061. (10.1002/2017GL074954)
53. Morlighem M, Rignot E, Binder T, Blankenship D, Drews R, Eagles G, Eisen O, Ferraccioli F, Forsberg R, Fretwell P, Goel V, Greenbaum JS, Gudmundsson H, Guo J, Helm V, Hofstede C, Howat I, Humbert A, Jokat W, Karlsson NB, Lee WS, Matsuoka K, Millan R, Mouginot J, Paden J, Pattyn F, Roberts J, Rosier S, Ruppel A, Seroussi H, Smith EC, Steinhage D, Sun B, van den Broeke MR, van Ommen TD, van Wessem M, Young DA. 2020 Deep Glacial Troughs and Stabilizing Ridges Unveiled beneath the Margins of the Antarctic Ice Sheet. *Nature Geoscience* **13**, 132–137. (10.1038/s41561-019-0510-8)
54. Morlighem M, Rignot E, Mouginot J, Seroussi H, Larour E. 2014 Deeply Incised Submarine Glacial Valleys beneath the Greenland Ice Sheet. *Nature Geoscience* **7**, 418–422. (10.1038/ngeo2167)
55. Goelzer H, Nowicki S, Edwards T, Beckley M, Abe-Ouchi A, Aschwanden A, Calov R, Gagliardini O, Gillet-Chaulet F, Golledge NR, Gregory J, Greve R, Humbert A, Huybrecht P, Kennedy JH, Larour E, Lipscomb WH, Leclec'h S, Lee V, Morlighem M, Pattyn F, Payne AJ, Rodehacke C, Ruckamp M, Saito F, Schlegel N, Seroussi H, Shepherd A, Sun S, van de Wal R, Ziemen FA. 2018 Design and Results of the Ice Sheet Model Initialisation Experiments initMIP-Greenland: An ISMIP6 Intercomparison. *Cryosphere* **12**, 1433–1460. (10.5194/tc-12-1433-2018)
56. Goelzer H, Nowicki S, Payne A, Larour E, Seroussi H, Lipscomb WH, Gregory J, Abe-Ouchi A, Shepherd A, Simon E, Agosta C, Alexander P, Aschwanden A, Barthel A, Calov R, Chambers C, Choi Y, Cuzzone J, Dumas C, Edwards T, Felikson D, Fettweis X, Golledge NR, Greve R, Humbert A, Huybrechts P, Le clec'h S, Lee V, Leguy G, Little C, Lowry DP, Morlighem M, Nias I, Quiquet A, Rückamp M, Schlegel NJ, Slater DA, Smith RS, Straneo F, Tarasov L, van de Wal R, van den Broeke M. 2020 The Future Sea-Level Contribution of the Greenland Ice Sheet: A Multi-Model Ensemble Study of ISMIP6. *The Cryosphere* **14**, 3071–3096. (10.5194/tc-14-3071-2020)
57. Seroussi H, Nowicki S, Payne AJ, Goelzer H, Lipscomb WH, Abe-Ouchi A, Agosta C, Albrecht T, Asay-Davis X, Barthel A, Calov R, Cullather R, Dumas C, Galton-Fenzi BK, Gladstone R, Golledge NR, Gregory JM, Greve R, Hattermann T, Hoffman MJ, Humbert A, Huybrechts P, Jourdain NC, Kleiner T, Larour E, Leguy GR, Lowry DP, Little CM, Morlighem M, Pattyn F, Pelle T, Price SF, Quiquet A, Reese R, Schlegel NJ, Shepherd A, Simon E, Smith RS, Straneo F, Sun S, Trusel LD, Van Breedam J, van de Wal RSW, Winkelmann R, Zhao C, Zhang T, Zwinger T. 2020 ISMIP6 Antarctica: A Multi-Model Ensemble of the Antarctic Ice Sheet Evolution over the 21st Century. *The Cryosphere* **14**, 3033–3070. (10.5194/tc-14-3033-2020)
58. Seroussi H, Verjans V, Nowicki S, Payne AJ, Goelzer H, Lipscomb WH, Abe-Ouchi A, Agosta C, Albrecht T, Asay-Davis X, Barthel A, Calov R, Cullather R, Dumas C, Galton-Fenzi BK, Gladstone R, Golledge NR, Gregory JM, Greve R, Hattermann T, Hoffman MJ, Humbert A, Huybrechts P, Jourdain NC, Kleiner T, Larour E, Leguy GR, Lowry DP, Little CM, Morlighem M, Pattyn F, Pelle T, Price SF, Quiquet A, Reese R, Schlegel NJ, Shepherd A, Simon E, Smith RS, Straneo F, Sun S, Trusel LD, Van Breedam J, Van Katwyk P, van de Wal RSW, Winkelmann R, Zhao C, Zhang T, Zwinger T. 2023 Insights into the Vulnerability of Antarctic Glaciers from the ISMIP6 Ice Sheet Model Ensemble and Associated Uncertainty. *The Cryosphere* **17**, 5197–5217. (10.5194/tc-17-5197-2023)

59. Seroussi H, Pelle T, Lipscomb WH, Abe-Ouchi A, Albrecht T, Alvarez-Solas J, Asay-Davis X, Barre JB, Berends CJ, Bernales J, Blasco J, Caillet J, Chandler DM, Coulon V, Cullather R, Dumas C, Galton-Fenzi BK, Garbe J, Gillet-Chaulet F, Gladstone R, Goelzer H, Golledge N, Greve R, Gudmundsson GH, Han HK, Hillebrand TR, Hoffman MJ, Huybrechts P, Jourdain NC, Klose AK, Langebroek PM, Leguy GR, Lowry DP, Mathiot P, Montoya M, Morlighem M, Nowicki S, Pattyn F, Payne AJ, Quiquet A, Reese R, Robinson A, Saraste L, Simon EG, Sun S, Twarog JP, Trusel LD, Urruty B, Van Breedam J, van de Wal RSW, Wang Y, Zhao C, Zwinger T. 2024 Evolution of the Antarctic Ice Sheet Over the Next Three Centuries From an ISMIP6 Model Ensemble. *Earth's Future* **12**, e2024EF004561. (10.1029/2024EF004561)
60. Morlighem M, Rignot E, Seroussi H, Larour E, Ben Dhia H, Aubry D. 2011 A Mass Conservation Approach for Mapping Glacier Ice Thickness. *Geophysical Research Letters* **38**. (10.1029/2011GL048659)
61. Morlighem M. 2022 MEaSUREs BedMachine Antarctica, Version 3. (10.5067/FPSU0V1MWUB6)
62. Roberts JL, Warner RC, Young D, Wright A, van Ommen TD, Blankenship DD, Siegert M, Young NW, Tabacco IE, Forieri A, Passerini A, Zirizzotti A, Frezzotti M. 2011 Refined Broad-Scale Sub-Glacial Morphology of Aurora Subglacial Basin, East Antarctica Derived by an Ice-Dynamics-Based Interpolation Scheme. *The cryosphere* **5**, 551–560. (10.5194/tc-5-551-2011)
63. MacKie EJ, Schroeder DM, Zuo C, Yin Z, Caers J. 2021 Stochastic Modeling of Subglacial Topography Exposes Uncertainty in Water Routing at Jakobshavn Glacier. *Journal of Glaciology* **67**, 75–83. (10.1017/jog.2020.84)
64. Matheron G. 1963 Principles of Geostatistics. *Economic Geology* **58**, 1246–1266. (10.2113/gsecongeo.58.8.1246)
65. Deutsch CV, Journel AG et al.. 1992 Geostatistical Software Library and User's Guide. *Oxford University Press* **8**, 0–1.
66. Mariethoz PG, Caers J. 2014 *Multiple-Point Geostatistics: Stochastic Modeling with Training Images*. John Wiley & Sons.
67. Yin Z, Zuo C, MacKie EJ, Caers J. 2022 Mapping High-Resolution Basal Topography of West Antarctica from Radar Data Using Non-Stationary Multiple-Point Geostatistics (MPS-BedMappingV1). *Geoscientific Model Development* **15**, 1477–1497. (10.5194/gmd-15-1477-2022)
68. Zuo C, Yin Z, Pan Z, MacKie EJ, Caers J. 2020 A Tree-Based Direct Sampling Method for Stochastic Surface and Subsurface Hydrological Modeling. *Water Resources Research* **56**, e2019WR026130. (10.1029/2019WR026130)
69. Nunes R, Soares A, Schwedersky G, Dillon L, Caetano H, Maciel C, Leon F. 2012 Geostatistical Inversion of Prestack Seismic Data. In *Ninth International Geostatistics Congress* pp. 1–8.
70. Reuschen S, Xu T, Nowak W. 2020 Bayesian Inversion of Hierarchical Geostatistical Models Using a Parallel-Tempering Sequential Gibbs MCMC. *Advances in Water Resources* **141**, 103614. (10.1016/j.advwatres.2020.103614)
71. Shamsipour P, Marcotte D, Chouteau M, Rivest M, Bouchedda A. 2013 3D Stochastic Gravity Inversion Using Nonstationary Covariances. *GEOPHYSICS* **78**, G15–G24. (10.1190/geo2012-0122.1)
72. Volkova A, Merkulov V. 2019 Iterative Approach of Gravity and Magnetic Inversion through Geostatistics. In *Petroleum Geostatistics 2019* vol. 2019 pp. 1–5. European Association of Geoscientists & Engineers. (10.3997/2214-4609.201902257)
73. Shao N, MacKie EJ, Field MJ, McCormack FS. 2025 A Markov chain Monte Carlo approach for geostatistically simulating mass-conserving subglacial topography. Manuscript under review (10.31223/X5SB2R)
74. Cai Y, He Y, Lang S, Cui X, Zhang X, Yao Z. 2025 Siamese Topographic Generation Model: A Deep Learning Model for Generating Antarctic Subglacial Topography with Fine Details. *Computers & Geosciences* **196**, 105857. (10.1016/j.cageo.2025.105857)
75. Leong WJ, Horgan HJ. 2020 DeepBedMap: A Deep Neural Network for Resolving the Bed Topography of Antarctica. *The Cryosphere* **14**, 3687–3705. (10.5194/tc-14-3687-2020)
76. Santhanam R, Raman S, Uzir N, Banerjee S. 2016 Experimenting XGBoost Algorithm for Prediction and Classification of Different Datasets. *International Journal of Control Theory and Applications* **9**, 651–662.
77. Yi K, Dewar A, Tabassum T, Lu J, Chen R, Alam H, Faruque O, Li S, Morlighem M, Wang J. 2023 Evaluating Machine Learning and Statistical Models for Greenland Subglacial Bed Topography. In *2023 International Conference on Machine Learning and Applications (ICMLA)* pp. 659–666. (10.1109/ICMLA58977.2023.00097)

78. Tapoglou E, Karatzas GP, Trichakis IC, Varouchakis EA. 2014 A spatio-temporal hybrid neural network-Kriging model for groundwater level simulation. *Journal of hydrology* **519**, 3193–3203.
79. Tyralis H, Papacharalampous G. 2024 A Review of Predictive Uncertainty Estimation with Machine Learning. *Artificial Intelligence Review* **57**, 94. (10.1007/s10462-023-10698-8)
80. Bingham RG, Vaughan DG, King EC, Davies D, Cornford SL, Smith AM, Arthern RJ, Brisbourne AM, De Rydt J, Graham AGC, Spagnolo M, Marsh OJ, Shean DE. 2017 Diverse Landscapes beneath Pine Island Glacier Influence Ice Flow. *Nature Communications* **8**, 1618. (10.1038/s41467-017-01597-y)
81. Rathmann NM, Lilien DA. 2022 Inferred Basal Friction and Mass Flux Affected by Crystal-Orientation Fabrics. *Journal of Glaciology* **68**, 236–252. (10.1017/jog.2021.88)
82. Brinkerhoff DJ, Aschwanden A, Truffer M. 2016 Bayesian Inference of Subglacial Topography Using Mass Conservation. *Frontiers in Earth Science* **4**. (10.3389/feart.2016.00008)
83. Choi Y, Petty A, Felikson D, Poterjoy J. 2025 Estimation of the State and Parameters in Ice Sheet Model Using an Ensemble Kalman Filter and Observing System Simulation Experiments. *EGUsphere* pp. 1–25. (10.5194/egusphere-2025-301)
84. Gillet-Chaulet F. 2020 Assimilation of Surface Observations in a Transient Marine Ice Sheet Model Using an Ensemble Kalman Filter. *The Cryosphere* **14**, 811–832. (10.5194/tc-14-811-2020)
85. Gudmundsson GH, Raymond M. 2008 On the Limit to Resolution and Information on Basal Properties Obtainable from Surface Data on Ice Streams. *The Cryosphere* **2**, 167–178. (10.5194/tc-2-167-2008)
86. Morlighem M, Goldberg D. 2023 Data Assimilation in Glaciology. In Ismail-Zadeh A, Castelli F, Jones D, Sanchez S, editors, *Applications of Data Assimilation and Inverse Problems in the Earth Sciences* , pp. 93–111. Cambridge University Press 1 edition. (10.1017/9781009180412.007)
87. Thorsteinsson T, Raymond CF, Gudmundsson GH, Bindschadler RA, Vornberger P, Joughin I. 2003 Bed Topography and Lubrication Inferred from Surface Measurements on Fast-Flowing Ice Streams. *Journal of Glaciology* **49**, 481–490. (10.3189/172756503781830502)
88. McArthur K, McCormack FS, Dow CF. 2023 Basal Conditions of Denman Glacier from Glacier Hydrology and Ice Dynamics Modeling. *The Cryosphere Discussions* pp. 1–29. (10.5194/tc-2023-28)
89. Wernecke A, Edwards TL, Holden PB, Edwards NR, Cornford SL. 2022 Quantifying the Impact of Bedrock Topography Uncertainty in Pine Island Glacier Projections for This Century. *Geophysical Research Letters* **49**, e2021GL096589. (10.1029/2021GL096589)
90. Gasson E, DeConto R, Pollard D. 2015 Antarctic Bedrock Topography Uncertainty and Ice Sheet Stability. *Geophysical Research Letters* **42**, 5372–5377. (10.1002/2015GL064322)
91. Sun S, Cornford SL, Liu Y, Moore JC. 2014 Dynamic Response of Antarctic Ice Shelves to Bedrock Uncertainty. *The Cryosphere* **8**, 1561–1576. (10.5194/tc-8-1561-2014)
92. Morlighem M, Goldberg D, Dias dos Santos T, Lee J, Sagebaum M. 2021 Mapping the Sensitivity of the Amundsen Sea Embayment to Changes in External Forcings Using Automatic Differentiation. *Geophysical Research Letters* **48**, e2021GL095440. (10.1029/2021GL095440)
93. Utke J, Naumann U, Fagan M, Tallent N, Strout M, Heimbach P, Hill C, Wunsch C. 2008 OpenAD/F: A Modular Open-Source Tool for Automatic Differentiation of Fortran Codes. *ACM Trans. Math. Softw.* **34**, 18:1–18:36. (10.1145/1377596.1377598)
94. Larour E, Seroussi H, Morlighem M, Rignot E. 2012 Continental Scale, High Order, High Spatial Resolution, Ice Sheet Modeling Using the Ice Sheet System Model (ISSM). *Journal of Geophysical Research: Earth Surface* **117**. (10.1029/2011JF002140)
95. Smith B, Fricker HA, Gardner AS, Medley B, Nilsson J, Paolo FS, Holschuh N, Adusumilli S, Brunt K, Csatho B, Harbeck K, Markus T, Neumann T, Siegfried MR, Zwally HJ. 2020 Pervasive Ice Sheet Mass Loss Reflects Competing Ocean and Atmosphere Processes. *Science* **368**, 1239–1242. (10.1126/science.aaz5845)
96. Rignot E, Mouginot J, Scheuchl B, van den Broeke M, van Wessem MJ, Morlighem M. 2019 Four Decades of Antarctic Ice Sheet Mass Balance from 1979–2017. *Proceedings of the National Academy of Sciences* **116**, 1095–1103.
97. Bird LA, McCormack FS, Beckmann J, Jones RS, Mackintosh AN. 2025 Assessing the Sensitivity of the Vanderford Glacier, East Antarctica, to Basal Melt and Calving. *The Cryosphere* **19**, 955–973. (10.5194/tc-19-955-2025)
98. Shepherd A, Ivins E, Rignot E, Smith B, van den Broeke M, Velicogna I, Whitehouse P, Briggs K, Joughin I, Krinner G, Nowicki S, Payne T, Scambos T, Schlegel N, A G, Agosta C, Ahlstrøm

A, Babonis G, Barletta V, Blazquez A, Bonin J, Csatho B, Cullather R, Felikson D, Fettweis X, Forsberg R, Gallee H, Gardner A, Gilbert L, Groh A, Gunter B, Hanna E, Harig C, Helm V, Horvath A, Horwath M, Khan S, Kjeldsen KK, Konrad H, Langen P, Lecavalier B, Loomis B, Luthcke S, McMillan M, Melini D, Mernild S, Mohajerani Y, Moore P, Mouginot J, Moyano G, Muir A, Nagler T, Nield G, Nilsson J, Noel B, Otosaka I, Pattle ME, Peltier WR, Pie N, Rietbroek R, Rott H, Sandberg-Sørensen L, Sasgen I, Save H, Scheuchl B, Schrama E, Schröder L, Seo KW, Simonsen S, Slater T, Spada G, Sutterley T, Talpe M, Tarasov L, van de Berg WJ, van der Wal W, van Wessem M, Vishwakarma BD, Wiese D, Wouters B, The IMBIE team. 2018 Mass Balance of the Antarctic Ice Sheet from 1992 to 2017. *Nature* **558**, 219–222. (10.1038/s41586-018-0179-y)

99. McCormack FS, Roberts JL, Kulessa B, Aitken A, Dow CF, Bird L, Galton-Fenzi BK, Hochmuth K, Jones RS, Mackintosh AN, McArthur K. 2023 Assessing the Potential for Ice Flow Piracy between the Totten and Vanderford Glaciers, East Antarctica. *The Cryosphere* **17**, 4549–4569. (10.5194/tc-17-4549-2023)
100. Rignot E, Mouginot J, Scheuchl B. 2011 Ice Flow of the Antarctic Ice Sheet. *Science* **333**, 1427–1430. (10.1126/science.1208336)
101. Rignot E, Mouginot J, Scheuchl B. 2017 MEaSUREs InSAR-based Antarctica Ice Velocity Map 450m V2.0. (10.5067/MEASURES/CRYOSPHERE/nsidc-0484.001)
102. Morlighem M, Seroussi H, Larour E, Rignot E. 2013 Inversion of Basal Friction in Antarctica Using Exact and Incomplete Adjoints of a Higher-Order Model. *Journal of Geophysical Research* **118**, 1746–1753. (10.1002/jgrf.20125)
103. Glen JW. 1952 Experiments on the Deformation of Ice. *Journal of Glaciology* **2**, 111–114.
104. Glen JW. 1953 Rate of Flow of Polycrystalline Ice. *Nature* **172**, 721–722.
105. Glen JW. 1955 The Creep of Polycrystalline Ice. *Proceedings of the Royal Society of London. Series A, Mathematical and Physical Sciences* **228**, 519–538.
106. Schoof C. 2005 The Effect of Cavitation on Glacier Sliding. *Proceedings of the Royal Society A* **461**, 609–627. (10.1098/rspa.2004.1350)
107. Schoof C. 2010 Coulomb Friction And Other Sliding Laws In A Higher-order Glacier Flow Model. *Math. Models Methods Appl. Sci.* **20**, 157–189. (10.1142/S0218202510004180)
108. Ehrenfeucht S, Morlighem M, Rignot E, Dow CF, Mouginot J. 2023 Seasonal Acceleration of Petermann Glacier, Greenland, From Changes in Subglacial Hydrology. *Geophysical Research Letters* **50**, e2022GL098009. (10.1029/2022GL098009)
109. Rignot E, Jacobs S, Mouginot J, Scheuchl B. 2013 Ice Shelf Melting around Antarctica. *Science (New York, N.Y.)* **341**, 266–270. (10.1126/science.1235798)
110. Jourdain NC, Asay-Davis X, Hattermann T, Straneo F, Seroussi H, Little CM, Nowicki S. 2020 A Protocol for Calculating Basal Melt Rates in the ISMIP6 Antarctic Ice Sheet Projections. *The Cryosphere* **14**, 3111–3134. (10.5194/tc-14-3111-2020)
111. Nowicki S, Goelzer H, Seroussi H, Payne AJ, Lipscomb WH, Abe-Ouchi A, Agosta C, Alexander P, Asay-Davis XS, Barthel A, Bracegirdle TJ, Cullather R, Felikson D, Fettweis X, Gregory JM, Hattermann T, Jourdain NC, Kuipers Munneke P, Larour E, Little CM, Morlighem M, Nias I, Shepherd A, Simon E, Slater D, Smith RS, Straneo F, Trusel LD, van den Broeke MR, van de Wal R. 2020 Experimental Protocol for Sea Level Projections from ISMIP6 Stand-Alone Ice Sheet Models. *The Cryosphere* **14**, 2331–2368. (10.5194/tc-14-2331-2020)
112. Vaňková I, Rintoul SR, Herraiz-Borreguero L, Silvano A, Greenbaum JS, van Ommen T, Jansen D, Blankenship DD. 2023 High Spatial Melt Rate Variability Near the Totten Glacier Grounding Line in East Antarctica. *Geophysical Research Letters* **50**, e2023GL102960. (10.1029/2023GL102960)
113. Aitken ARA, Roberts JL, van Ommen TD, Young DA, Golledge NR, Greenbaum JS, Blankenship DD, Siegert MJ. 2016 Repeated Large-Scale Retreat and Advance of Totten Glacier Indicated by Inland Bed Erosion. *Nature* **533**, 385–389. (10.1038/nature17447)
114. Pelle T, Morlighem M, McCormack FS. 2020 Aurora Basin, the Weak Underbelly of East Antarctica. *Geophysical Research Letters* **47**. (10.1029/2019GL086821)
115. Sun S, Cornford SL, Gwyther DE, Gladstone RM, Galton-Fenzi BK, Zhao L, Moore JC. 2016 Impact of Ocean Forcing on the Aurora Basin in the 21st and 22nd Centuries. *Annals of Glaciology* **57**, 79–86. (10.1017/aog.2016.27)
116. Ehrenfeucht S, Dow CF. 2025 Impacts of bed topography resolution on sea-level rise projections from coupled subglacial hydrology and ice dynamics for Thwaites Glacier, West Antarctica. Manuscript in preparation.

117. Badgeley JA, Morlighem M, Seroussi H. 2025 Increased Sea-Level Contribution from Northwestern Greenland for Models That Reproduce Observations. *Proceedings of the National Academy of Sciences* **122**, e2411904122. (10.1073/pnas.2411904122)
118. Höyns LS, Kleiner T, Rademacher A, Rückamp M, Wolovick M, Humbert A. 2025 Improved basal drag of the West Antarctic Ice Sheet from L-curve analysis of inverse models utilizing subglacial hydrology simulations. *The Cryosphere* **19**, 2133–2158. (10.5194/tc-19-2133-2025)
119. Wolovick M, Humbert A, Kleiner T, Rückamp M. 2023 Regularization and L-curves in ice sheet inverse models: a case study in the Filchner–Ronne catchment. *The Cryosphere* **17**, 5027–5060. (10.5194/tc-17-5027-2023)
120. Weertman J. 1957 On the Sliding of Glaciers. *Journal of Glaciology* **3**, 33–38. (10.3189/S0022143000024709)
121. Zoet LK, Iverson NR. 2020 A Slip Law for Glaciers on Deformable Beds. *Science* **368**, 76–78. (10.1126/science.aaz1183)
122. McCormack FS, Roberts JL, Dow CF, Stål T, Halpin JA, Reading AM, Siegert MJ. 2022 Fine-Scale Geothermal Heat Flow in Antarctica Can Increase Simulated Subglacial Melt Estimates. *Geophysical Research Letters* **49**, e2022GL098539. (10.1029/2022GL098539)
123. Reading AM, Stål T, Halpin JA, Lösing M, Ebbing J, Shen W, McCormack FS, Siddoway CS, Hasterok D. 2022 Antarctic Geothermal Heat Flow and Its Implications for Tectonics and Ice Sheets. *Nature Reviews Earth & Environment* **3**, 814–831. (10.1038/s43017-022-00348-y)
124. Smith-Johnsen S, Schlegel NJ, de Fleurian B, Nisancioglu KH. 2020 Sensitivity of the Northeast Greenland Ice Stream to Geothermal Heat. *Journal of Geophysical Research: Earth Surface* **125**. (10.1029/2019JF005252)
125. Thoma M, Mayer C, Grosfeld K. 2008 Sensitivity of Subglacial Lake Vostok's Flow Regime on Environmental Parameters. *Earth and Planetary Science Letters* **269**, 242–247. (10.1016/j.epsl.2008.02.023)
126. Bougamont M, Christoffersen P, Price SF, Fricker HA, Tulaczyk S, Carter SP. 2015 Reactivation of Kamb Ice Stream Tributaries Triggers Century-Scale Reorganization of Siple Coast Ice Flow in West Antarctica. *Geophysical Research Letters* **42**, 8471–8480. (10.1002/2015GL065782)

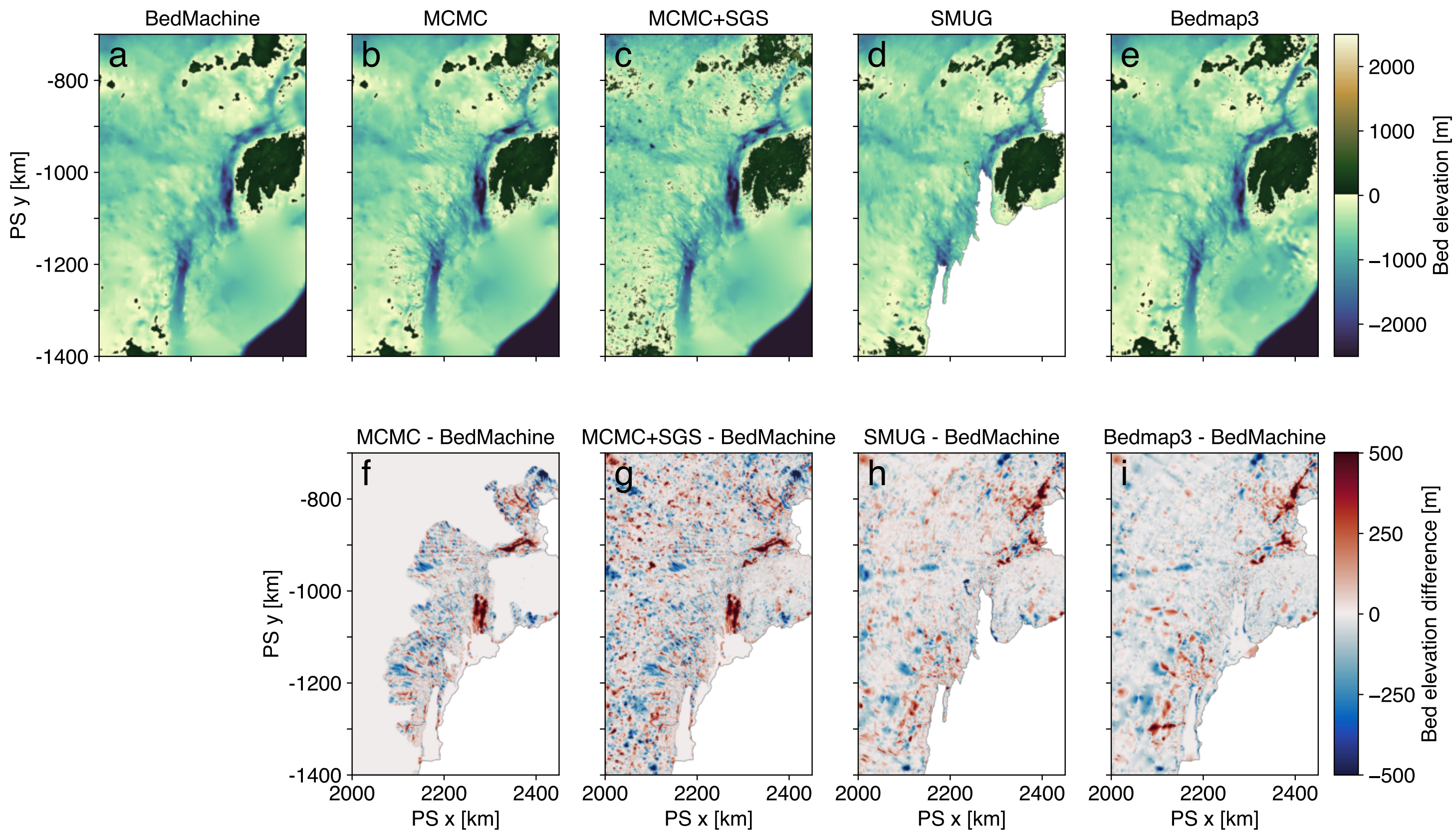

Figure 2. Bed elevation datasets (m) considered in our Aurora Subglacial Basin ensemble, zoomed into the Totten-MUIS region, as follows: (a) BedMachine [53]; (b) MCMC [73]; (c) MCMC with SGS conditioned based on MCMC (MCMC+SGS); (d) SMUG [46]; and (e) Bedmap3 [44]. Differences between the BedMachine dataset and the MCMC, MCMC+SGS, SMUG and Bedmap3 datasets are shown in panels (f)-(i).

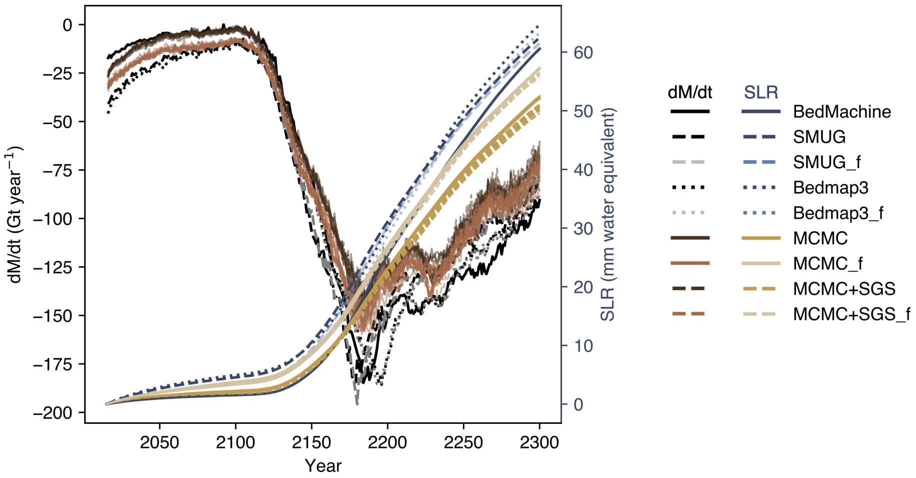

Figure 3. Rate of change of ice mass above flotation (dM/dt, Gt year^{-1}; darker curves and the left y-axis) and sea level rise (SLR, mm water equivalent; lighter curves and the right y-axis) from simulations of the Aurora Subglacial Basin to 2300 CE. The spread between the scenarios with the BedMachine Antarctica, SMUG, Bedmap3, MCMC, and MCMC+SGS beds is shown for scenarios that use the friction coefficient derived from inversion using the BedMachine bed versus friction coefficients derived from inversion using each individual bed realisation other than BedMachine (simulations with an _f suffix).

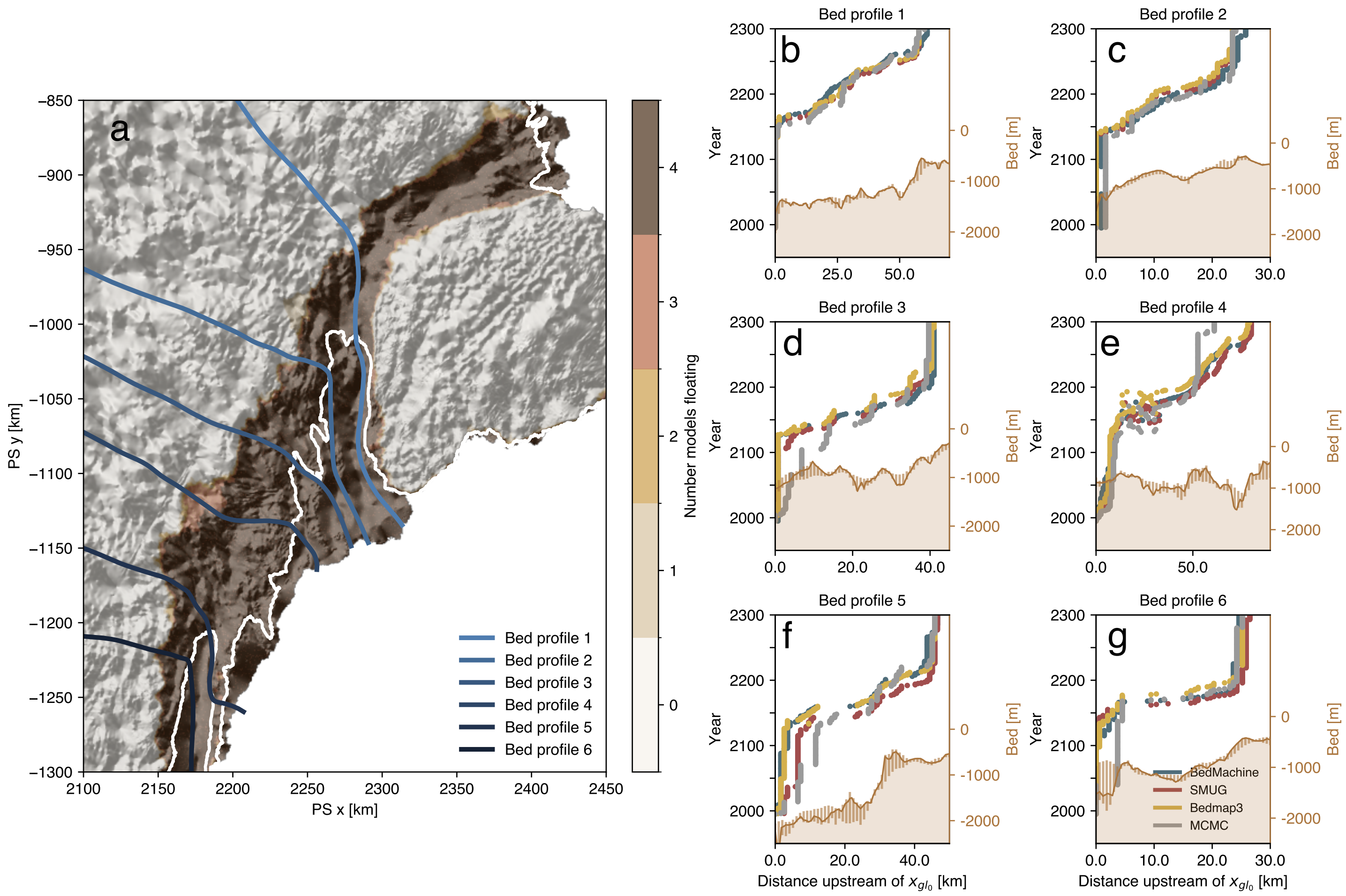

Figure 4. (a) Shading shows the number of ensemble members that predict floating ice in the region of the Totten and MUIS Glaciers on a background hillshade model of BedMachine v3 Antarctica, with the white line designating the present-day grounding line position [53]. Six streamlines are shown (blue lines), which correspond to the profiles in panels (b)-(g). The median of the BedMachine, SMUG, Bedmap3, MCMC, and MCMC+SGS beds is shown (solid brown line; right y-axis), with the range (minimum to maximum of all bed realisations) indicated by vertical lines. The grounding line retreat over time for the BedMachine, SMUG, Bedmap3, and one MCMC bed realisation is shown in coloured dotted lines (left y-axis).